Article

Cell Reports

The WD40 Protein BamB Mediates Coupling of BAM Complexes into Assembly Precincts in the Bacterial Outer Membrane

Graphical Abstract

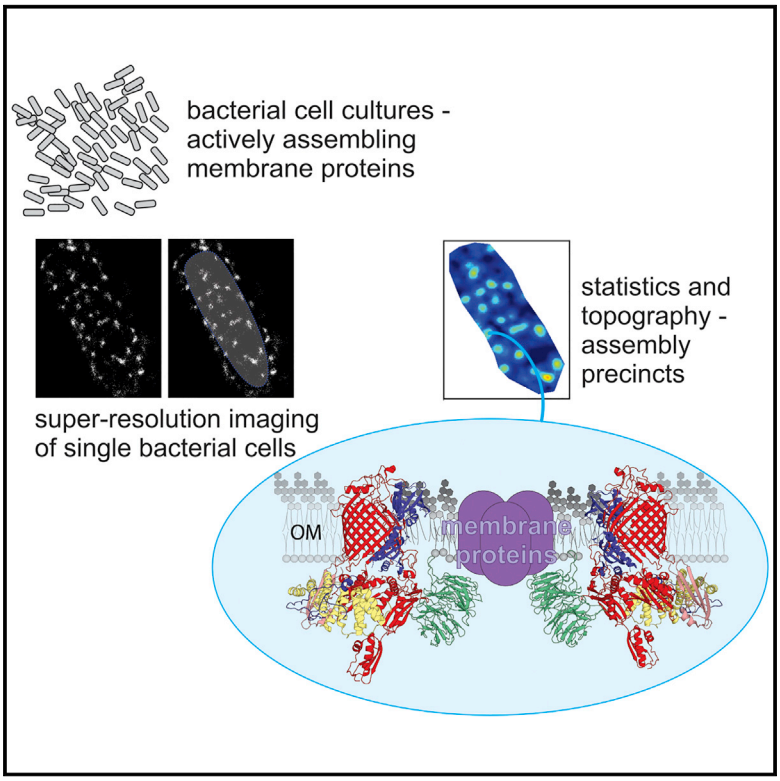

Authors

Sachith D. Gunasinghe, Takuya Shiota, Christopher J. Stubenrauch, ..., Kirstin D. Elgass, Richard A. Strugnell, Trevor Lithgow

Correspondence

trevor.lithgow@monash.edu

In Brief

Bacteria grow and divide by assembling new material into their surface membranes. Gunasinghe et al. used super-resolution microscopy and *in situ* crosslinking in live bacterial cells in order to visualize intimate contacts between BAM complexes suggesting a model whereby bacteria use highly organized precincts to drive membrane protein assembly.

Highlights

- Several BAM complexes sit together in an assembly precinct
- Assembly precincts are distributed right across the bacterial cell surface
- The BamB and BamA subunits mediate BAM-BAM interactions
- Assembly precincts potentiate porin trimerization by neigboring BAM complexes

Gunasinghe et al., 2018, Cell Reports *23*, 2782–2794
May 29, 2018
https://doi.org/10.1016/j.celrep.2018.04.093

CellPress

OPEN ACCESS
CellPress

Cell Reports
Article

The WD40 Protein BamB Mediates Coupling of BAM Complexes into Assembly Precincts in the Bacterial Outer Membrane

Sachith D. Gunasinghe,[1,9] Takuya Shiota,[1,2,9] Christopher J. Stubenrauch,[1] Keith E. Schulze,[3] Chaille T. Webb,[1] Alex J. Fulcher,[1,3,4] Rhys A. Dunstan,[1] Iain D. Hay,[1] Thomas Naderer,[4] Donna R. Whelan,[5,6] Toby D.M. Bell,[5] Kirstin D. Elgass,[3,7] Richard A. Strugnell,[8] and Trevor Lithgow[1,10,*]

[1]Infection & Immunity Program, Biomedicine Discovery Institute, and Department of Microbiology, Monash University, Clayton, VIC 3800, Australia
[2]Organization for Promotion of Tenure Track, University of Miyazaki, Miyazaki 889-1692, Japan
[3]Monash Micro Imaging, Monash University, Clayton, VIC 3800, Australia
[4]Infection & Immunity Program, Biomedicine Discovery Institute, and Department of Biochemistry & Molecular Biology, Monash University, Clayton, VIC 3800, Australia
[5]School of Chemistry, Monash University, Clayton, VIC 3800, Australia
[6]Department of Biochemistry and Molecular Pharmacology, New York University School of Medicine, New York, NY, USA
[7]Hudson Institute of Medical Research, Clayton, VIC 3800, Australia
[8]Department of Microbiology & Immunology, University of Melbourne, Parkville, VIC 3052, Australia
[9]These authors contributed equally
[10]Lead Contact
*Correspondence: trevor.lithgow@monash.edu
https://doi.org/10.1016/j.celrep.2018.04.093

SUMMARY

The β-barrel assembly machinery (BAM) complex is essential for localization of surface proteins on bacterial cells, but the mechanism by which it functions is unclear. We developed a direct stochastic optical reconstruction microscopy (dSTORM) methodology to view the BAM complex *in situ*. Single-cell analysis showed that discrete membrane precincts housing several BAM complexes are distributed across the *E. coli* surface, with a nearest neighbor distance of ~200 nm. The auxiliary lipoprotein subunit BamB was crucial for this spatial distribution, and *in situ* crosslinking shows that BamB makes intimate contacts with BamA and BamB in neighboring BAM complexes within the precinct. The BAM complex precincts swell when outer membrane protein synthesis is maximal, visual proof that the precincts are active in protein assembly. This nanoscale interrogation of the BAM complex *in situ* suggests a model whereby bacterial outer membranes contain highly organized assembly precincts to drive integral protein assembly.

INTRODUCTION

In Gram-negative bacteria, the outer membrane is the external surface of the cell. Transmembrane β-barrel proteins constitute a major fraction of the mass of this outer membrane, performing roles that range from passive diffusion of simple nutrients to a range of virulence-specific traits. The assembly of these proteins depends on a set of factors that constitute the β-barrel assembly machinery (BAM), the major and essential component of which is the core BAM complex (Hagan et al., 2011; O'Neil et al., 2015). The catalytic function of the BAM complex depends on an essential subunit, BamA (Bakelar et al., 2016; Gu et al., 2016; Han et al., 2016; Noinaj et al., 2013), but the precise mechanism by which the BAM complex assembles β-barrel proteins into the bacterial outer membrane remains to be elucidated (Gessmann et al., 2014; Noinaj et al., 2013, 2014).

The architecture of the BAM complex is understood from crystal structures of the individual components: BamA (Noinaj et al., 2013), the WD40 protein BamB (Heuck et al., 2011; Kim and Paetzel, 2011; Noinaj et al., 2011), the helix-grip protein BamC (Kim et al., 2011), the tetratricopeptide-repeat protein BamD (Kim et al., 2011; Sandoval et al., 2011) and BamE (Knowles et al., 2011), and BAM complex oligomers (Bakelar et al., 2016; Bergal et al., 2016; Gu et al., 2016; Han et al., 2016; Malinverni et al., 2006; Rigel et al., 2012; Vuong et al., 2008). Our current understanding is that each BamA molecule interacts with one molecule of each of the other BAM subunits, with BamC exposed on the outer face of the outer membrane and BamB, BamD, and BamE exposed to the periplasm (Hagan et al., 2011; O'Neil et al., 2015). The BAM complex has been proposed to directly fold substrate proteins strand by strand (Noinaj et al., 2014), while other studies suggest that the BAM complex may create a local, non-bilayer lipid environment to lower the activation energy of substrate protein insertion into the outer membrane (Gessmann et al., 2014). These elements of BAM complex activity in the process of outer membrane biogenesis are still under study, and the two different propositions are not mutually exclusive.

In terms of bacterial cell biology, there are two conflicting models concerning the spatially important aspects of outer

membrane protein biogenesis during cell growth. One of these models (Rassam et al., 2015) was based on total internal reflection fluorescence microscopy (TIRFM) analysis and molecular dynamics simulations on two abundant β-barrel proteins, BtuB and Cir. This study concluded that the BAM complex inserts β-barrel proteins only at a spatially constrained zone at the midpoint of the cell, and only thereafter do outer membrane proteins move toward the cell poles. Conversely, Theriot and colleagues monitored the appearance of nascent molecules of LamB, using *in situ* labeling to record the initial breaching of this β-barrel protein outwardly through the outer membrane (Ursell et al., 2012). Statistical analyses of the confocal imaging data suggested that the sites of insertion for LamB were randomly distributed across the outer membrane of *E. coli*, not restricted to the midpoint of the cells (Ursell et al., 2012). On the assumption that LamB insertion sites in the outer membrane represent the position of the BAM complex, a random distribution across the outer membrane surface (Ursell et al., 2012) is at odds with a midline-specific localization of active BAM complexes (Rassam et al., 2015).

Given these differing conclusions on how and where β-barrel proteins are inserted into the outer membrane, we sought to directly assess the spatial distribution of the BAM complex in intact *E. coli* cells, isolated from log-phase cultures where nascent protein flux into the outer membrane would be maximal. For this spatial assessment of the BAM complex, we utilized new developments in super-resolution imaging technology to interrogate bacterial cell biology at nanoscale resolution (Gahlmann and Moerner, 2014). BAM complexes were visualized in precincts, studded around the cells with nearest neighbor distances of ~200 nm between them. We use the term "precincts" by definition of an area designated for specific or restricted use and to be consistent with the emerging trend of functionally restricted domains in bacterial membranes (Strahl and Errington, 2017). Each of the protein assembly precincts contains multiple BAM complexes, and interaction between the BAM complexes was shown to be mediated by the BamB subunit: *in situ* crosslinking demonstrated the interactive residues of BamB mediating these contacts, while in the absence of BamB, the precincts disperse. Since the diameter of the assembly precincts shrinks ~20% in the absence of nascent OMP substrates, we conclude that these assembly precincts are actively engaged in outer membrane biogenesis.

RESULTS

The BAM Complex Is Organized into Assembly Precincts

The BAM complex is a nanomachine that spans the outer membrane (Figure 1A) with a maximal diameter across the periplasmic portion of ~10 nm (Gu et al., 2016; Han et al., 2016; O'Neil et al., 2015). As it is the defining subunit of the BAM complex, antibodies specific for the POTRA domains of BamA were used as probes to address the distribution of the BAM complex across the bacterial surface. Titration experiments were undertaken with detergents to provide limited permeabilization of the lipid phase of the outer membrane, sufficient to allow access of the antibodies into the periplasm. Control experiments showed that treatment with 0.001% digitonin was sufficient to allow an externally added protein reagent (Proteinase K) into the periplasm, as judged by proteolysis of proteins in that compartment (Figure S1A). This treatment also provided antibody access to detect the distribution of BamA by dSTORM. Spatial distribution analyses of BamA showed speckles of protein across the cell surface (Figure 1B). We developed algorithms and a workflow to analyze and describe the spatial distribution parameters of BAM complex locations (Figures 1C and S2A). The parameter L(r) − r was derived (Supplemental Experimental Procedures) as a means to plot BAM complex distributions ($L(r)-r$ versus r) that would distinguish random distribution (which coincide with the x axis of the plot) from organized distributions. Thus, plots of L(r) − r versus r show the radius of a circle in which the highest degree of clustering can be observed (Figure 1C), and the cluster density figures showed 13.54 ± 0.4 sites per square micrometer of cellular surface (Figure 1D; Table S6).

For reasons defined later, we refer to these sites as assembly precincts. The mean diameter of the precincts was calculated as 130.2 ± 9.1 nm (Figure 1D). Given the size of the antibody probes used for detection, the mean diameter of the fluorescence image cannot be used to determine the diameter of the BAM complexes in each of these precincts. In a broad approximation, however, the number of each BAM subunit is ~300 per cell (Wiśniewski and Rakus, 2014), the average surface area is up to 6 μm^2 for an *E. coli* cell (Sundararaj et al., 2004), and the number of BAM precincts observed by dSTORM imaging is ~13 per μm^2 (Figure 1D), suggesting that there are several BAM complexes located in each assembly precinct.

BamC is expressed on the surface of *E. coli* (Webb et al., 2012a), as judged by immunofluorescence staining (Figure 2A). This provided a means to use dSTORM for super-resolution imaging of *E. coli* to detect the distribution of the BAM complex without permeabilizing the cells. A Δ*bamC* strain of *E. coli* in which the *bamC* gene was deleted served as a control to validate the immunofluorescence as specific to BamC. Importantly, treatment of wild-type *E. coli* with or without 0.001% digitonin did not significantly change the distribution of BamC (Figure S1C; Table 1; Table S6). Across the bacterial cell surface, dSTORM imaging of BamC demonstrated a distribution similar to that seen for BamA (Figure 2B; Table 1). In compiling the measurements from multiple (n = 53) cells, this distribution was uniform along the length of the *E. coli* cells (Figure 2C). To generate a three-dimensional view of the BamC distribution on the cell surface, a Vutara 350 imaging system was also used for three-dimensional single-molecule localization microscopy (Juette et al., 2008; Mlodzianoski et al., 2009). These scans confirmed that the precincts are distributed all across the surface of the *E. coli* cell, with no concentration at mid-point or polar regions (Figure 2D).

At log phase, the synthesis and trafficking of proteins destined to the cell surface is maximal in order to maintain rapid cell growth and division. As a result, the flux of proteins from the periplasm into the outer membrane would also be maximal. If the precincts seen in log-phase *E. coli* represent BAM complexes actively engaged in outer membrane protein assembly, the diameter of the precinct would be, in part, due to the bulk contributed by the substrates undergoing assembly and might

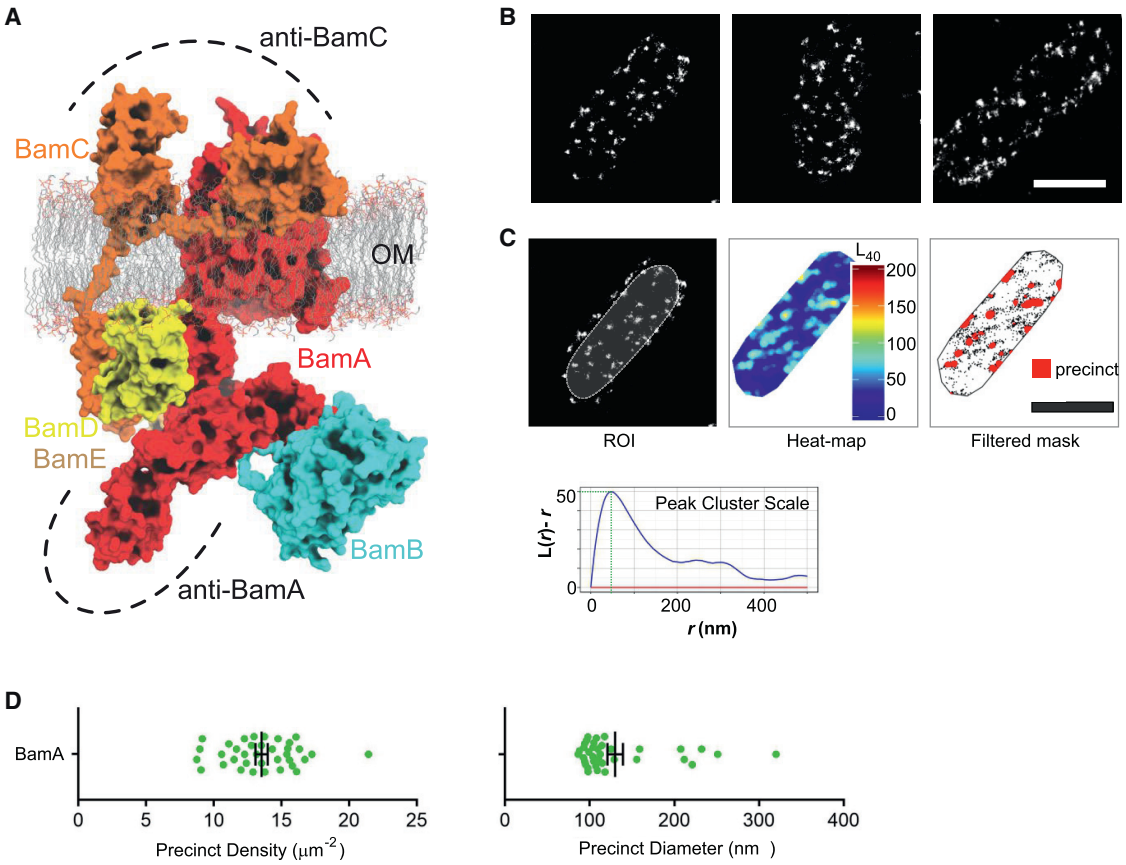

Figure 1. Spatial Distribution of BamA across the Surface of Detergent-Solubilized *E. coli*

(A) Topology of the BAM complex, with POTRA domains contained within the periplasm, requiring the addition of detergent to allow the access of labeling probes. BamC traverses the outer membrane (OM) (Webb et al., 2012a; O'Neil et al., 2015).

(B) Reconstructed dSTORM imaging of BamA for three individual *E. coli* cells. Scale bar, 1 μm.

(C) (Top left) dSTORM reconstructed super-resolution image showing the region of interest (ROI), (top middle) heatmap generated for the corresponding area, (top right) edge effects filtered binary mask showing thresholding for precinct analysis and (bottom) the peak cluster scale graph showing the radius in which the highest numbers of precincts occurs. Scale bar, 1 μm. See the Experimental Procedures and Figure S2A for details.

(D) Measurements showing BamA average (left) precinct density and (right) diameter in detergent-treated *E. coli* cells. Error bars represent mean ± SEM. Further statistical analysis is provided in Table S6.

See also Figure S2 and Table S6.

diminish in the absence of ongoing protein synthesis. To test whether this reduction in the diameter of the BAM complex precincts could be visualized by dSTORM, rifampicin was used to block transcription. With transcription blocked, the synthesis of outer membrane proteins is blocked as judged with a pulse of ^{35}S-amino acids (Figure 3A; Stenberg et al., 2007; Stubenrauch et al., 2016), so that subsequent assembly into membranes is halted. To be certain that rifampicin does not affect cell viability through the course of the experiment, a Live-Dead dual-staining protocol was used. Both live and dead bacterial cells take up the green stain SYTO9, but only dead cells are permeable to propidium iodide and so also stain red, as is seen in the heat-treated control cells (Figure 3B). While Live-Dead staining of *E. coli* after 60 min of rifampicin treatment showed no effect on cell viability (Figure 3B), imaging of these rifampicin-treated cells (Figure 3C) demonstrated a decrease in size of BAM complex precincts: in the absence of ongoing protein synthesis, the average diameter and area are diminished by ~20% (Figure 3C, bottom; Table S6). Ipso facto, the size of protein assembly precincts is expanded by the presence of nascent protein substrates.

BamB Is Crucial to the Interaction of BAM Complexes

Structurally, BamB is a WD40 protein (Heuck et al., 2011; Jansen et al., 2015; Kim and Paetzel, 2011; Noinaj et al., 2011), and WD40 β-propeller structures can serve to hold together unit complexes into super-complexes, such as is seen in the coatomer coat around secretory vesicles (Miller, 2013) and the membrane-attached lattice of the nuclear pore complex (Leksa and Schwartz, 2010). In each of these archetypal arrays, the WD40 protein subunits make both heterotypic and homotypic interactions in order to stabilize the larger structure. Therefore, we sought to address the hypothesis that the WD40 protein BamB functions to organize BAM complexes into precincts in the bacterial outer membrane.

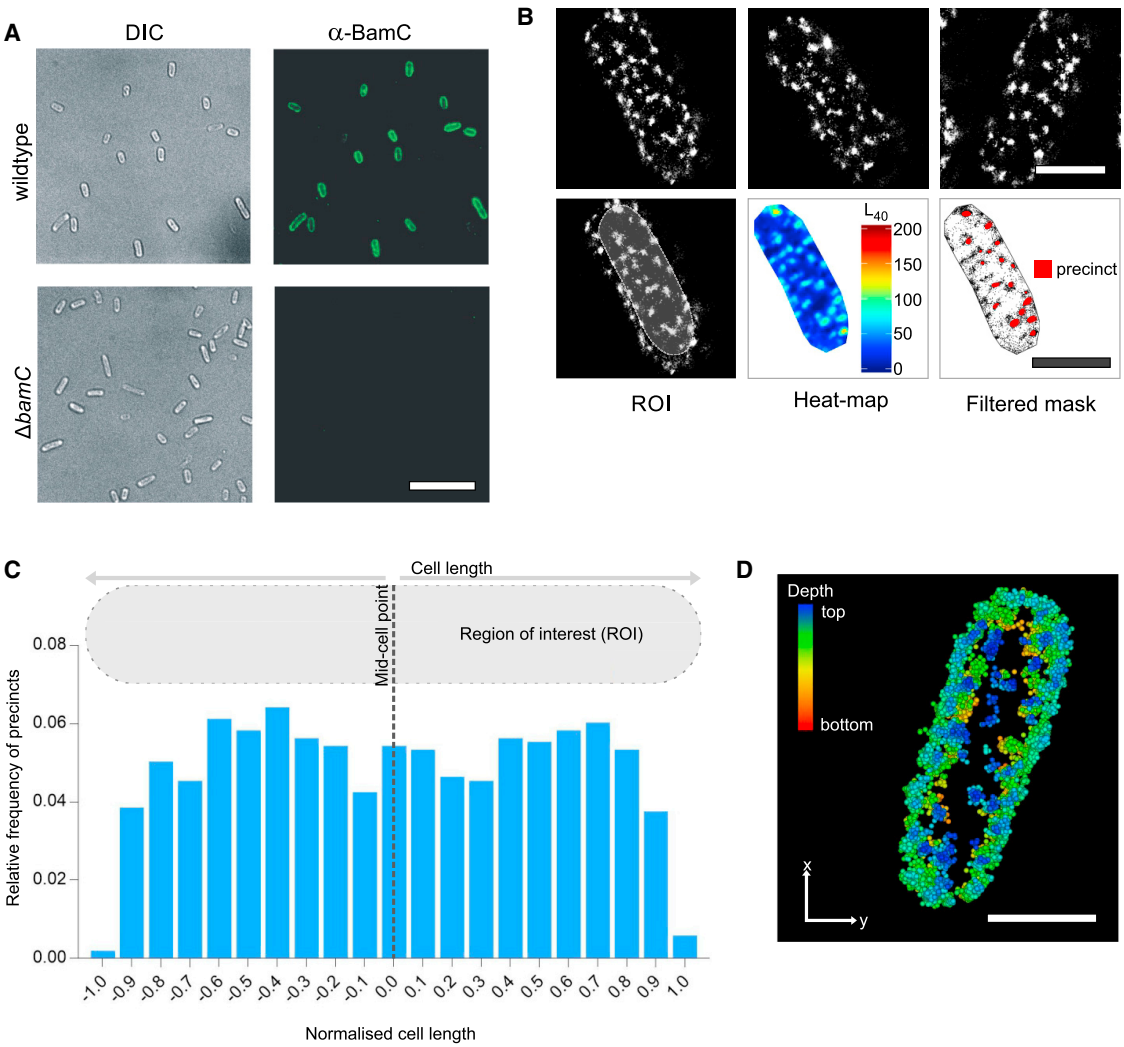

Figure 2. Spatial Distribution of BamC across the Surface of *E. coli*

(A) Immunofluorescence assessment of *E. coli* using antibodies recognizing BamC: differential interference contrast (DIC) image (left) for a representative field of cells and fluorescence image of antibody staining (right). Also shown is the isogenic Δ*bamC* mutant. Scale bar, 10 μm.

(B) Upper panel: dSTORM images of BamC distribution in representative *E. coli* cells. Lower panel: the region of interest (ROI), the corresponding heatmap, and filtered binary mask are shown (Figure S2A).Scale bars, 1 μm.

(C) The relative frequency of precincts along the cell length. Data are compiled from n = 53 cells. The procedure developed for the mapping of BAM complex distributions along the cell length is described in the Experimental Procedures.

(D) Surface distribution of BamC revealed by three-dimensional single-molecule localization super-resolution imaging. This representative image of a single cell has been immune-stained to detect BamC, with single-probe immunofluorescence shown in the "x,y" dimension, colored by the depth of the signal in the z-dimension. Scale bar, 1 μm.

See also Figure S2.

We define as the orthodox binding face of the disc-shaped BamB (Figures 4A and S3) the surface that interacts with BamA in crystal structures (Figure 4B). Sequence conservation analysis revealed that the interfacial residues of BamB on this orthodox face are highly conserved, yet so too are residues on the lateral edges and "unorthodox" face of BamB (Figures 4A and S4). To capture interactions between BamB and BamA *in situ*, crosslinking was established in live bacterial cells. Amber stop-codons were introduced at 31 positions in *bamA* (Figure S5A). In these strains, *p*-benzoyl-L-phenylalanine (BPA) residues are inserted at the amber codon, providing for UV-activated cross-linking to neighboring subunits within 4 Å (Farrell et al., 2005; Wittelsberger et al., 2008). Synthesis of BPA-containing BamA was driven by the *bamA* promoter in a strain of *E. coli* engineered to have the endogenous *bamA* repressed by glucose (Dunstan et al., 2015; Lehr et al., 2010). Bacterial cells were harvested in log phase, when outer membrane biogenesis is most active, and then UV-irradiated to induce crosslinking.

Several cross-link products were identified in the region corresponding to POTRA domains P1 and P4, but these do not

Table 1. BamA and BamC Distribution Statistics

Detection	Sample Size(n)	Average Precinct Density (μm^{-2})	Average Mean Precinct Area (nm^2)	Average Nearest Neighbor Distances(nm)
BamA (0.001% digitonin)	46	13.54 ± 0.4	6,363 ± 278.7	175.3 ± 5.2
BamC (no detergent)	53	10.94 ± 0.4	7,801 ± 221.2	220.4 ± 6.0
BamC (0.001% digitonin)	77	11.56 ± 0.3	7,074 ± 202.5	211.1 ± 4.2

Averages ± SEM for precinct density, mean precinct area, and nearest neighbor distances between precincts are calculated for BamA and BamC (an extended version is given in Table S6).

correspond to interactions with BamB (Figure S5B). At least one position, V^{76}, is cross-linked to the molecular chaperone SurA (Figure S5B), validating that the *in situ* analysis is capturing physiologically relevant interactions, given that this interaction has been reported previously (Bennion et al., 2010). The interactions with BamB were mapped to BPA-substituted residues in the BamA POTRA domain P3 (Figure 4C). This interaction, cross-linked in the outer membrane environment, is consistent with contacts between BamB and BamA in the crystal structure of the BAM complex (Gu et al., 2016; Han et al., 2016; Jansen et al., 2015). To test for reciprocity, BPA residues were inserted into various positions in BamB (Figure S3B), highlighting positions in the orthodox face of BamB, such as S^{193} or L^{244} (Figure 4D), that are in contact with BamA.

The "unorthodox face" of BamB is defined as the surface that is presented radially in a way that does not allow for intra-complex contacts but that could potentially allow contacts between neighboring BAM complexes (Figures 4B and S3). This possibility was tested. BPA residues at positions K^{90} and D^{138} of BamB were found to be cross-linked to BamA (Figure 4D). Based on the architecture of a single BAM complex (Figure 4B), this result requires that BamB mediates an interaction with a neighboring BAM complex. Given the potential importance of this result, and the way in which WD40 proteins interact in both homotypic and heterotypic ways to form super-complexes (Leksa and Schwartz, 2010; Miller, 2013), we sought to test the observation by introducing cysteine residues into BamB to test for BamB-BamB interactions.

The periplasm has an oxidizing environment that allows for neighboring cysteine residues to form disulfide bonds. We determined two positions in BamB: K^{90} and D^{138}, where the introduction of a cysteine residue caused the modified BamB to migrate on SDS-PAGE at sizes consistent with those of cross-linked species. In the case of BamB(K^{90}C), formation of the cross-linked species was accentuated in the presence of an oxidizing agent (Figure 4E). To be certain that these were disulfide-linked species, a sample of the membranes was subject to reducing conditions by addition of DTT, which reduced the disulfide linkage liberating BamB from the cross-linked species (Figure 4F). On SDS-PAGE, only linear polypeptides migrate according to their predicted molecular weight, with cross-linked species migrating aberrantly, due to the various conformations they adopt. Protein mass spectrometry analysis of affinity-purified cross-link species revealed BamB to be predominantly present in the samples BamB(K^{90}C) and BamB(D^{138}C), with the most commonly identified other proteins being contaminants from the cytoplasm, such as DnaK and KatE, and cytoplasmic membrane MgtA (Table S7). These data strongly suggest that these are BamB-BamB linkages mediated through the unique cysteine introduced at positions K^{90} and D^{138}.

The absence of BamB has no effect on the growth rate of *E. coli* on rich medium (Figure 5A). The absence of BamB impacts neither on the steady-state levels of its partner subunits of the BAM complex (Figure 5B) nor on the integrity of the BAM complex, as judged by blue-native (BN)-PAGE (Figure 5C) or X-ray crystallography (Noinaj et al., 2016). Thus, it was significant that dSTORM imaging of these *ΔbamB* mutants (Figure 5D) showed a loss of precinct localizations of the BAM complex in the absence of BamB (Figure 5E). There is a significant difference in both the precinct density and the proportion of BAM complexes found in precincts in the *ΔbamB* mutants (Figures 5E and S6). The average precinct area for the BAM complex is diminished from 7,801 ± 221 nm^2 (wild-type) to 4,232 ± 353 nm^2 (*ΔbamB*), and only 26% of BAM complexes are found in these smaller remnant localizations in the absence of BamB (Table S6).

Further support for the proximity of BAM complexes in the outer membrane came from "closed-gate" alleles of *bamA*. In probing the mechanism of BamA function, intramolecular disulfide-induced cross-links have been used to close the lateral gate (Figure 5F) between β strand 1 and β strand 16 of the β-barrel domain of BamA (Noinaj et al., 2014). In our studies on one of these mutants, BamA($G^{433}C/N^{805}C$), we observed the reduced ($BamA_{(red)}$) and oxidized ($BamA_{(ox)}$) forms of the protein (Figure 5F, upper panel), as previously described (Noinaj et al., 2014). However, longer exposures of the immunoblots invariably showed a disulfide-linked BamA oligomer, suggesting that two molecules of BamA had formed an intermolecular disulfide bond (Figure 5F, lower panel). Consistent with the observation that BamB is crucial to keep BAM complexes in close proximity, very little of the intermolecular cross-linked species was observed in *ΔbamB* mutant cells (Figure 5F).

An Assay System to Measure OmpC Trimerization

A classic assay for measuring membrane protein assembly into canine pancreatic microsomes was developed by Warren and Dobberstein (1978). We adapted the principles of this assay to interrogate specific rate-limiting steps in an otherwise complex membrane biogenesis pathway. Using optimized steps in cell disruption by sonication and isolation by rapid high-speed centrifugation (Figure 6A), a membrane fraction that we refer to as *E. coli* microsomal membranes (EMMs) can be collected that was found to be competent to drive the trimerization of β-barrel proteins such as OmpC.

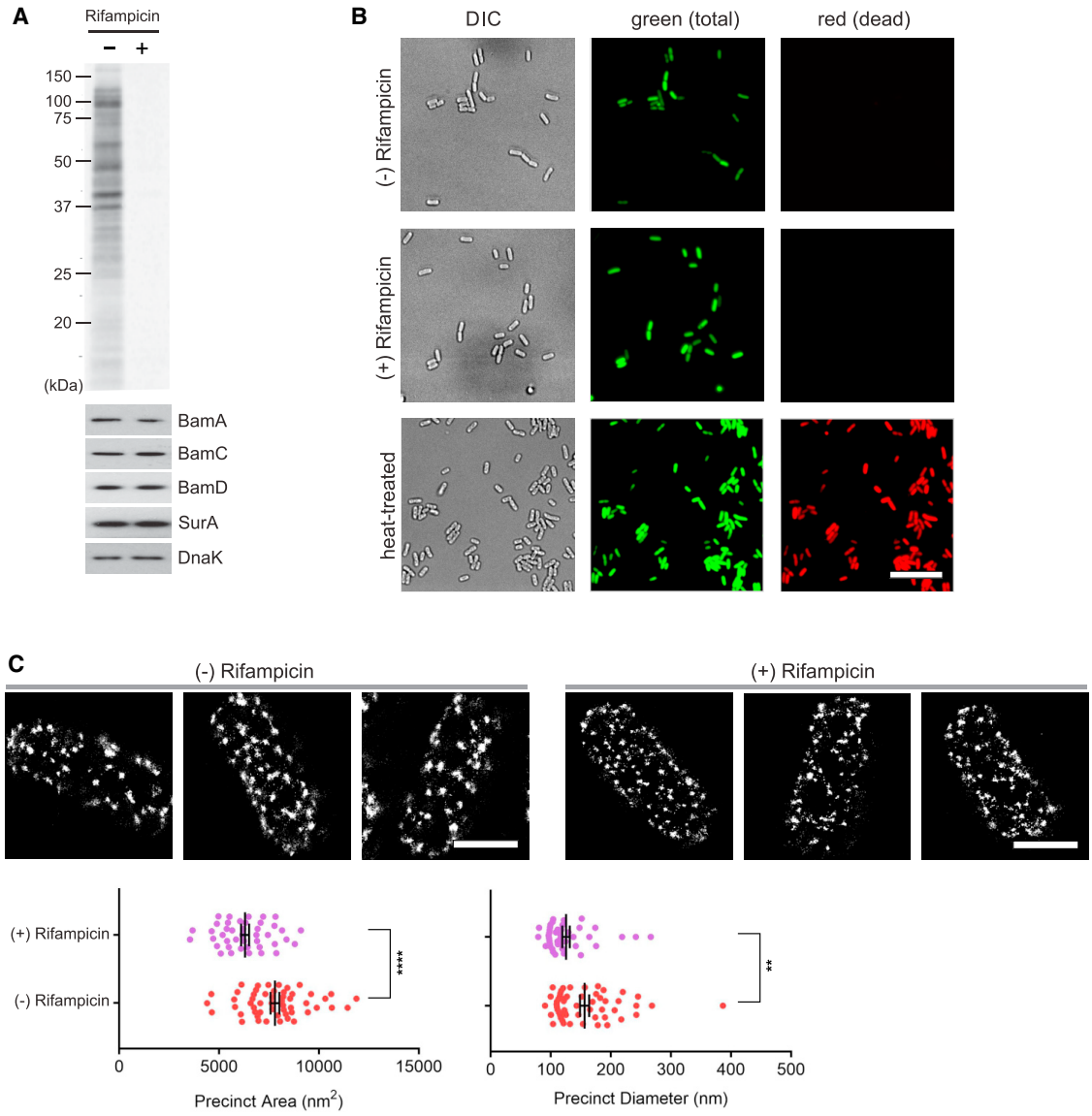

Figure 3. BAM Complex Precinct Diameters Are Greater with Ongoing Protein Synthesis

(A) *E. coli* subject to preincubation with (+) or without (–) rifampicin were subsequently labeled with ^{35}S to measure protein synthesis. Cell extracts (50 μg total protein) were analyzed by SDS-PAGE and storage phosphor imaging (upper panel) to measure ongoing protein synthesis or immunoblotting (lower panel) to determine the steady-state levels of the indicated proteins.

(B) Live-Dead staining of *E. coli* after rifampicin treatment for 60 min. As a control, a sample of cells was incubated at 90°C. Green indicates all cells; red indicates dead cells. Scale bar, 10 μm.

(C) Upper panel: dSTORM super-resolution images of BamC distribution with and without rifampicin treatment. Scale bars, 1 μm. Lower panels: graphs show BAM complex distribution statistics, with comparisons of significance reported using an unpaired t test (**$p \leqslant 0.01$; ****$p \leqslant 0.0001$). Error bars represent mean ± SEM.

The major porin OmpC was prepared as a substrate by *in vitro* translation in the presence of radioactive label ([^{35}S]-methionine and [^{35}S]-cysteine). BN-PAGE analysis showed that [^{35}S]-labeled OmpC was assembled into oligomers over time (Figure 6B). Given that they are the largest species (~160 kDa) and form at later time points (~30 min), we labeled the largest oligomers of OmpC as trimers. The assembly reaction that is monitored here was dependent on the EMM fraction (Figure 6B), and, to be certain that this was a BAM-complex-mediated assembly reaction, we assayed membranes from a strain of *E. coli* in which the activity of the BAM complex is compromised by a BamA(AAA) mutation (Figures S7D–S7F). There is an inhibition of the OmpC oligomers in the microsomal membranes prepared from this *bamA* mutant and a complete loss of assembly in an EMM fraction prepared from the *bamA*-deficient mutant strain with a control plasmid (i.e., without *bamA* present; Figure 6C).

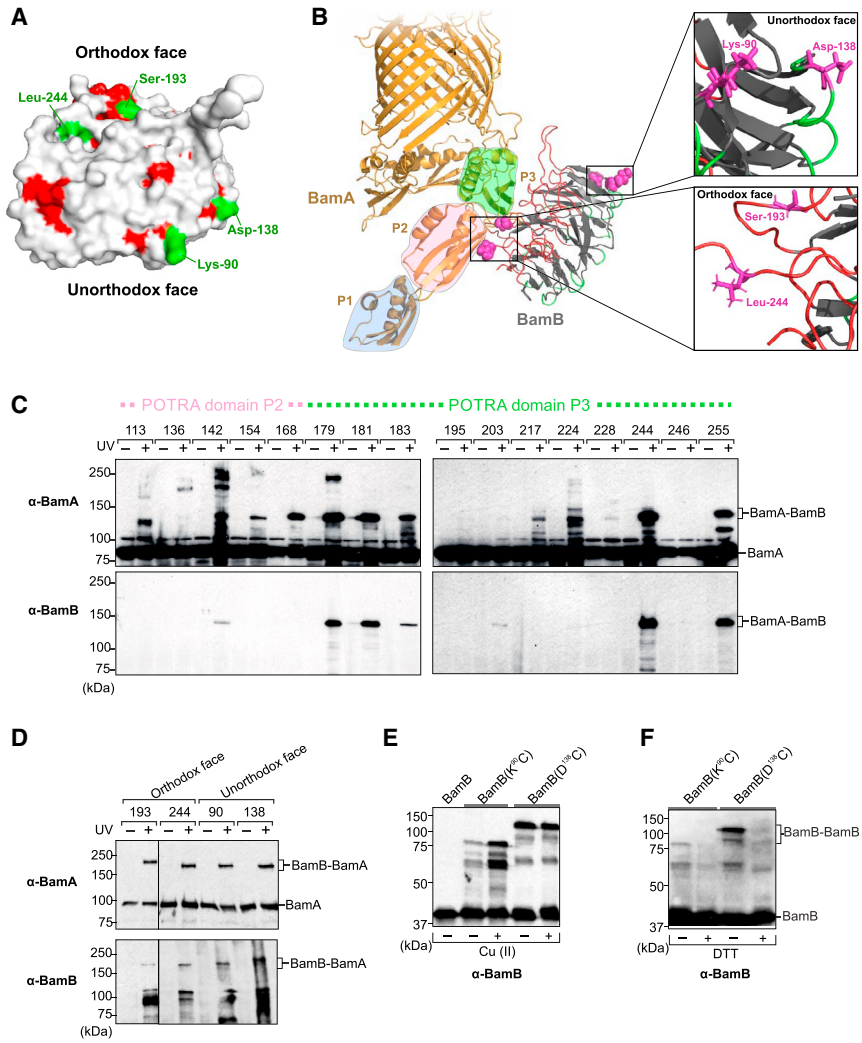

Figure 4. The WD40 Protein BamB Cross-links BAM Complexes in the Outer Membrane

(A) Structure of BamB (PDB: 3p1l) shaded to indicate conserved residues (Albrecht and Zeth, 2011). Analysis of sequence conservation is included in Figure S4.

(B) Structure of BamAB (PDB: 5d0o) indicates the positions of BPA residues inserted into BamB (represented by purple spheres). Inter-strand loops in the orthodox face and unorthodox face of BamB are shaded in red and green, respectively. Inset: a closer look at the orthodox face residues S^{193} and L^{244} and unorthodox face residues K^{90} and D^{138}.

(C) BamA(BPA) alleles from positions 113 to 255 spanning POTRA domains P2 to P3. In each case, membrane samples were subjected (+) or not subjected (–) to UV irradiation, solubilized in detergent for nickel-affinity purification, and then analyzed by SDS-PAGE and immunoblotting with antibodies specific for BamA or BamB. The migration of molecular weight standards is indicated in kilodaltons.

(D) *In situ* crosslinking of BamB(BPA) alleles to BamA was determined as indicated above.

(E) *E. coli* (Δ*bamB* mutants) were transformed with pGEM-T plasmids encoding BamB, BamB($K^{90}C$), or BamB($D^{138}C$) and subjected to *in situ* cross-linking. The identity of the BamB-BamB cross-link products was determined by mass spectrometry (Table S7) after immunblotting failed to detect any other Bam subunits in the cross-link products. Samples were treated with (+) or without (–) copper (II) sulfate to accentuate the oxidizing conditions that would drive disulfide cross-links.

(F) *In situ* crosslinking of BamB cys-cys alleles; samples were treated with (+) or without (–) DTT in order to reduce the disulfide cross-links.

See also Figure S4 and Table S7.

With the parameters of the assay system optimized, it was used to address the question of whether assembly precincts of BAM complexes are important for generating the trimeric species of the major porin. Monitoring the assembly of [^{35}S]-labeled OmpC in Δ*bamB* mutants showed that BamB is required for rapid trimerization of the nascent OmpC molecules (Figure 6D). In the presence of BamB, by 30 min, the assembled trimer represents the major species of OmpC, whereas at this same time point, 75% of the OmpC is yet to be assembled (Figure S7H). While the EMM assay system measures a combined impact on insertion into the membrane and assembly into the trimer, there is at least a substantial impact on trimerization rates in the absence of BamB.

DISCUSSION

In recent years, there have been great advances in studying membrane proteins by X-ray crystallography and cryoelectron microscopy (cryo-EM) (Seeger, 2017). Because these structures can only be solved from purified proteins that are not in a native membrane environment, we know that many aspects of their structure will not be captured and must instead be modeled using computational tools (Almeida et al., 2017). In parallel, the growing awareness that bacterial membranes are not uniform but can have functionally distinguishable domains (Strahl and Errington, 2017) requires new approaches to study the spatial organization of membrane proteins. In this study on the BAM complex, we used super-resolution imaging of intact *E. coli* cells in conjunction with *in situ* crosslinking in intact *E. coli* to demonstrate an organization of BAM complexes into areas that we refer to as the assembly precinct, a nanoscale area designated for the purpose of β-barrel protein assembly and integration.

The concept of a membrane super-complex is not new, at least not in eukaryotic cell biology. Arguably, the best understood of these are the respiratory chain super-complexes found in the mitochondrial inner membrane (Milenkovic et al., 2017). These super-complexes have precise arrangements of complexes, which dissociate when membranes are solubilized with detergent and X-ray crystallography of the individual parts built a jigsaw-like picture that was ultimately pieced together. We

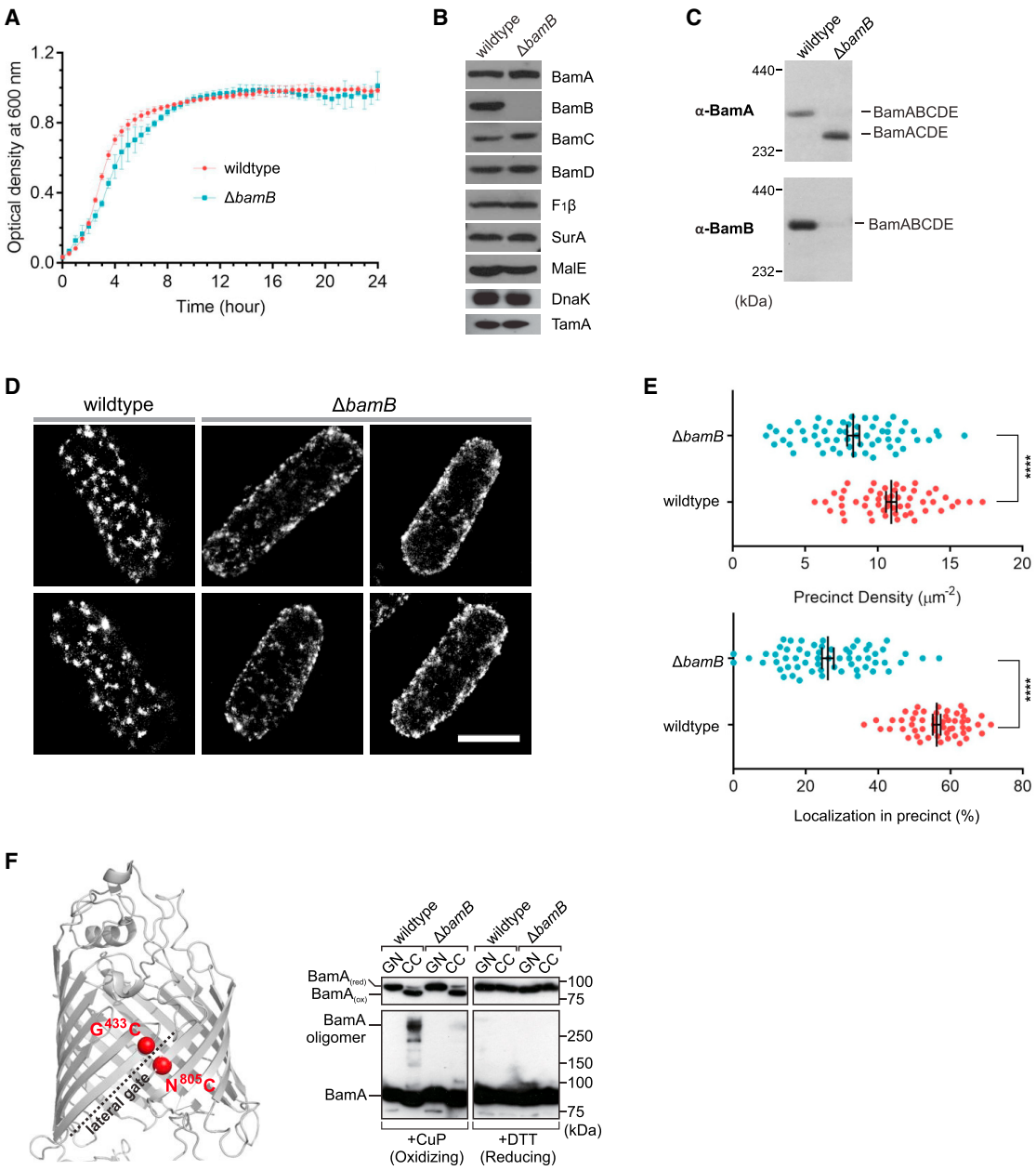

Figure 5. BamB Is Required to Maintain Assembly Precinct Interactions in the Outer Membrane

(A) Growth curves for *E. coli* and the isogenic Δ*bamB* mutant. Samples were taken at intervals and assessed by spectrophotometry. Error bars represent mean ± SD from four independent experiments (n = 4).

(B) Total cell extracts from the wild-type *E. coli* and the isogenic Δ*bamB* mutant were subjected to SDS-PAGE and immunoblotting with the indicated antisera (outer membrane protein TamA, periplasmic proteins SurA and MalE, inner membrane protein $F_1\beta$, and cytoplasmic protein DnaK).

(C) Membrane extracts from wild-type *E. coli* and the isogenic Δ*bamB* mutants were subjected to BN-PAGE and immunoblotting with antiserum recognizing BamA (upper panel) and BamB (lower panel). The migration position for the molecular size markers is indicated.

(D) dSTORM imaging of wild-type *E. coli* and the Δ*bamB* mutants, using anti-BamC for detection. Scale bar, 1 μm.

(E) Spatial analysis for the BAM complex distribution in the Δ*bamB* mutants. Data for precinct density and percentage of localization in precincts are shown, with the full analysis shown in Figure S6 and Table S6. Comparisons of significance are reported using unpaired t test (****$p \leqslant 0.0001$). Error bars represent mean ± SEM.

(F) Position of G^{433} in the first transmembrane β strand of BamA and N^{805} in the last β strand of BamA (left panel). Total cell extracts were prepared from *E. coli* expressing BamA ("GN"), or the disulfide-forming version carrying $G^{433}C$ and $N^{805}C$ replacements in BamA ("CC"), analyzed by SDS-PAGE and immunoblotting with antibodies recognizing BamA. The upper panel shows a short exposure of the immunoblot that distinguishes the oxidized and reduced forms of BamA, as previously described (Noinaj et al., 2014). The lower panel is a longer exposure, indicating the ~200- to 250-kDa oligomer of BamA.

See also Figure S6 and Table S6.

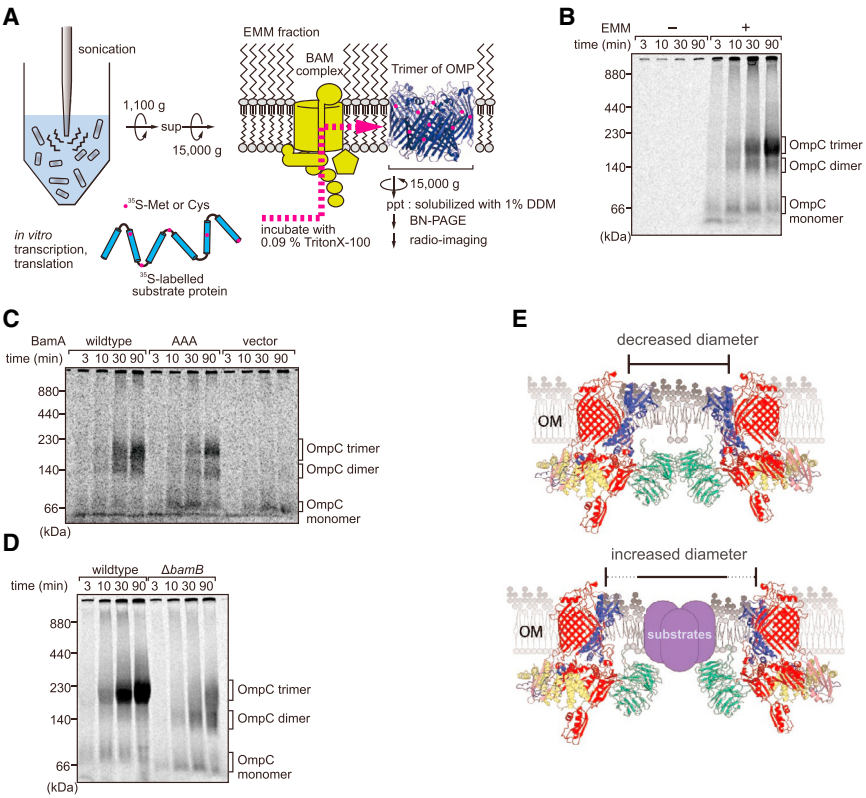

Figure 6. A Bacterial Outer Membrane Microsomal Assay to Measure OMP Trimerization

(A) Depiction of the assay for assembly of ^{35}S-labeled OmpC into oligomers, as detailed in the Experimental Procedures. DDM, dodecylmaltoside.

(B) ^{35}S-labeled OmpC was translated *in vitro* and incubated with (+) or without (–) the EMM fraction. At the indicated time points, the EMM fraction was harvested by high-speed centrifugation and analyzed by BN-PAGE.

(C) Mutation of three highly conserved residues (R^{661}, G^{662}, and F^{663}) in loop 6 of BamA to three alanine residues severely affects BAM complex function (Rigel et al., 2012). EMM fractions isolated from *E. coli* harboring either native *bamA* ("wildtype"), the AAA mutant of *bamA* (AAA), or a control plasmid ("vector") were incubated with ^{35}S-OmpC, and assembly was analyzed by BN-PAGE and storage phosphor imaging.

(D) EMM isolated from wild-type *E. coli* or the isogenic *ΔbamB* mutant, incubated with ^{35}S-labeled OmpC. At the indicated time points, the EMMs were harvested by high-speed centrifugation and analyzed by BN-PAGE and storage phosphor imaging. Analysis of the data by densitometry is provided in Figure S7H.

(E) Diagram illustrating the change in diameter of the assembly precinct by virtue of the presence or absence of incoming substrates handled by the multiple BAM complexes in the precinct. OM, outer membrane.

See also Figure S7.

have not determined here whether the assembly precinct is a super-complex: the arrangement of BAM complexes may be strict and ordered within the precinct, but it might, alternatively, be a less geometric arrangement of BAM complexes. Recent crystal structures of the individual BAM complex with and without the BamB subunit (Bakelar et al., 2016; Bergal et al., 2016; Gu et al., 2016; Han et al., 2016) have built a great deal of knowledge on how the subunits are arranged relative to each other and are inspiring ideas about the mechanism driving β-barrel protein assembly into the outer membrane (Albenne & Ieva, 2017; Noinaj et al., 2017; Plummer & Fleming, 2016). However, several questions have remained. How are trimeric outer membrane proteins built, given that each BAM complex appears to mediate assembly of a single β-barrel? How closely linked to the passage of unfolded nascent chains across the inner membrane is the BAM-complex-mediated assembly into the outer membrane? What is the specific function of each of the non-essential lipoproteins in the BAM complex?

That *bamB* is ubiquitously present in the genomes of other alpha-, beta-, and gamma-proteobacterial lineages argues that the function of BamB is important (Webb et al., 2012b). However, observations that Δ*bamB* mutants are viable and grow at similar rates to wild-type *E. coli* in rich medium in the laboratory argues that the proximity of BAM complexes is neither essential nor rate limiting to cell growth under these conditions, obscuring the specific function of BamB until now.

BamA is essential for integration of each polypeptide into the membrane, which necessarily also has an impact on assembly. In a previous study, BamB was shown to have an impact on the assembly of an autotransporter catalyzed by the BAM complex (Ieva et al., 2011). Whether BamB also plays a direct role in the assembly of the monomer, or, perhaps, whether the precinct it helps to form shields a distinct lipid environment that assists the assembly process (and that would be lost in the absence of BamB), will require a different experimental approach and has not yet been addressed. Here, we show in an assay directed specifically at dissecting the insertion of the substrate into the membrane from the assembly reaction that generates the final trimeric form of the substrate, that BamB can exert an impact on the oligomerization of β-barrel proteins. We suggest that this occurs as a result of the clear role that BamB plays in promoting the existence of assembly precincts.

Three pieces of evidence support the conclusion that the assembly precincts observed here are functionally relevant. First, their size diminishes when substrate proteins are no longer entering the outer membrane (Figure 6E). The size of the antibody reagents used for detection of the BAM complexes does not allow us to use the magnitude of the diameter to calculate any meaningful parameter of the precinct, but a percent change in the diameter is meaningful. Second, distribution of the assembly precincts across the *E. coli* cell is consistent with the distribution of sites of emergence for LamB substrate molecules onto the cell surface in *E. coli* (Ursell et al., 2012). The third piece of evidence is an EMM fraction prepared from a Δ*bamB* mutant: where the other BAM subunits are present at wild-type amounts and where they remain associated in BamACDE complexes that

are not in precincts are compromised in their ability to oligomerize the substrate protein OmpC. The EMM assay is a means to bypass other, rate-limiting, steps such as those mediated by SecYEG, SurA, etc., which lead up to the interaction of substrates such as OmpC with the BAM complex. Taken in the context of the spatial distribution of BAM complexes seen in intact *E. coli* ± BamB, we suggest that the proximity of BAM complexes is an important feature in fostering the delivery of each integrated monomer of OmpC to its partners in order to most effectively constitute the functional form of the protein in the outer membrane.

The *in situ* crosslinking approach promises some answers toward a fuller understanding of the assembly precinct: the molecular chaperone SurA was identified interacting with the BamA POTRA domain P1 (the present study), and a chaperone-protease called BepA can also be cross-linked to BamA, BamC, and BamD by this approach (Daimon et al., 2017). At this early stage, it is unclear whether the assembly precincts also contain other membrane-embedded modules of the β-barrel assembly machinery, such as the TAM (Albenne & Ieva, 2017; Noinaj et al., 2017). It is also unclear whether the BAM complexes are kept in the vicinity of SecYEG complexes, which appear to be of somewhat lower abundance than the BAM complex (Lycklama a Nijeholt and Driessen, 2012) yet have recently been suggested to be to be in close proximity to the BAM complex (Wang et al., 2016). The technology and analytical methodology are now available to address whether spatial arrangements coordinate and protect the passage of nascent polypeptides from the cytoplasm to the outer membrane for folding into β-barrel proteins.

EXPERIMENTAL PROCEDURES

Bacterial Strains and Plasmids

Unless otherwise indicated, all experiments were performed using *E. coli* BW25113 wild-type or Δ*bamB*. *E. coli* BW25113 Δ*bamB* was obtained from the Keio collection (Baba et al., 2006) and validated by PCR and immunoblotting. Plasmids and primers used in this study are described in Tables S2 and S3, respectively.

Growth Conditions and Sample Preparation for Microscopy

Cells were grown to mid-log phase in LB media (Miller) at 37°C with shaking (200 rpm). Then 500 μL of cells were subjected to centrifugation (4,000 × g, 5 min, 4°C), washed twice in PBS, and resuspended in 500 μL PBS. The 8-well, coverglass-bottom chambers (Sarstedt) were coated with 0.01% (v/v) poly-L-lysine (Sigma-Aldrich) for 10 min at room temperature before excess poly-L-lysine was removed. Afterward, 200 μL *E. coli* cells were immobilized onto each coated well chamber. To ensure a monolayer of bacteria was formed, chamber slides were subjected to centrifugation (4,000 × g, 3 min, 4°C) and washed three times with PBS. The monolayer of bacteria was then fixed with a mixture of paraformaldehyde (2% w/v) and glutaraldehyde (0.2% v/v) in PBS for 5 min at 4°C, which was then washed in PBS to remove excess fixatives. Auto-fluorescence was minimized with the addition of freshly prepared 0.1% (w/v) $NaBH_4$ in PBS for 15 min, followed by two washing steps of PBS (Clancy and Cauller, 1998). Where applicable, the samples were permeabilized either with digitonin (0.001% w/v in PBS) or Triton X-100 (0.001% v/v in PBS), followed by three washing steps with PBS.

In experiments where rifampicin pretreatment was used, *E. coli* cells were grown to mid-log phase in LB media (Miller), and native protein transcription was sufficiently inhibited by the addition of rifampicin (200 μg/mL) followed by 1 hr incubation at 37°C with vigorous shaking (200 rpm). Live-cell sample preparation was carried out using 8-well, coverglass-bottom chambers (Sarstedt) as described earlier. Prior to cellular fixation, live-dead staining of *E. coli* cells was performed using the LIVE/DEAD BacLight Bacterial Viability Kit from Molecular Probes. Dead-cell controls were prepared using heat treatment (Li et al., 2014). An Olympus IX-81 inverted fluorescence microscope equipped with Olympus Cell^M software was used to visualize cell samples using the 100× objective with fluorescein isothiocyanate (FITC) and tetramethylrhodamine (TRITC) filters.

Growth Curves

Four independent colonies of *E. coli* wild-type or Δ*bamB* were individually used to inoculate LB liquid media (Miller). Cells were incubated overnight (30°C, 200 rpm [25-mm orbit]). Samples were diluted in fresh media of the same composition to an optical density at 600 nm (OD_{600}) of 0.05, and 200 μL of each sample was loaded into a 96-well plate. OD_{600} was automatically measured at 30-min intervals (over 24 hr) using the Tecan Spark 10M multimode microplate reader (30°C, 180 rpm [3.0-mm orbit]).

Primary and Secondary Antibody Labeling

Validity of primary antibodies was confirmed by the usage of corresponding genomic knockouts from the Keio collection in western blots and in immunofluorescence microscopy. Primary and secondary antibodies used in this study are listed in Table S1. Blocking was performed with 5% w/v BSA in PBS for 1 hr at room temperature, followed by incubation of antibodies diluted to 1:1,000 in 5% w/v BSA in PBS for 1-hr mixing by rotary inversion at room temperature. The primary antibodies were then removed, and the wells were washed twice with PBS followed by the addition of secondary anti-mouse/anti-rabbit immunoglobulin G (IgG)-Alexa Fluor 647 (Thermo Fisher Scientific)-conjugated antibody diluted to 1:1,000 in 5% BSA in PBS for 45 min at room temperature. The secondary antibody was then removed, and the wells were washed twice with PBS before the samples were stored at 4°C in PBS prior to microscopy imaging.

Assessment of Membrane Integrity by Access to Proteinase K

E. coli wild-type cells were grown to mid-log phase (OD_{600} of about 0.6) in LB media. Fifty microliters of cells were harvested by centrifugation (4,000 × *g*, 5 min) before resuspending the cell pellet in 500 μL TBS. Digitonin (0.001% w/v) or polymyxin B (500 μg/mL) was added to cells as required and incubated at 4°C on a rotary wheel for 15 min. Proteinase K (200 μg/mL) was subsequently added to cells and incubated at 4°C for up to 60 min. At the indicated time points, trichloroacetic acid (10% v/v) was added, and samples were incubated on ice for 30 min. Protein pellets were washed twice in acetone (25,000 × *g*, 20 min), air dried, and resuspended in 50 μL SDS sample buffer. Samples (35 μL) were analyzed by SDS-PAGE and immunoblotting for BamA (1:10,000), BamC (1:20,000), BamD (1:20,000), and SurA (1:10,000).

dSTORM Super-resolution Microscopy Setup

Super-resolution (SR) images were recorded on a custom-built dSTORM setup using an Olympus IX-71 base equipped with the appropriate fluorescence filter cubes, a 488-nm Toptica laser (200 mW), a 561-nm Laser Quantum laser (500 mW), a 638-nm Oxxius laser (150 mW), an Olympus UPlanSApo Uis2 oil-immersion 100× NA 1.4 objective, a 1.6× magnification changer engaged, and an Andor iXon Ultra 897 high-speed electron multiplying charge-coupled device (EMCCD) camera with single-photon sensitivity for single-molecule detection. The final excitation steering mirror and beam expansion lenses were mounted on a translation stage for free adjustment of the TIRF angle. The system was operated at a TIRF angle appropriate for the respective sample to concentrate excitation power and reduce background fluorescence. Samples were mounted on a manual x,y translation stage to minimize sample drift.

Imaging Buffer Preparation

SR on Alexa Fluor 647-labeled samples were performed in an imaging buffer consisting of TN buffer (50 mM Tris-HCL [pH 8.0], 10 mM NaCl), oxygen scavenger system GLOX (0.5 mg/mL glucose oxidase, G2133, Sigma-Aldrich; 40 μg/mL catalase, C-100, Sigma-Aldrich; and 10% w/v glucose), and 10 mM 2-aminoethanethiol (MEA: M6500, Sigma-Aldrich). MEA was made as a 1-M stock solution in 50 mM Tris buffer, with a pH adjusted to 8.0 using

KOH. MEA aliquots were stored at −20°C and thawed immediately before use. GLOX was stored at 4°C.

Software for Analysis of dSTORM Imaging

Details of the imaging analysis methodology are provided in the Supplemental Experimental Procedures. Source code for an automated version of the analysis procedure described here is hosted as a Git repository and is available at https://github.com/monashmicroimaging/autoclustr.

Mapping BAM Complex Distributions along the Cell Length

The distribution of BAM clusters along the length axis of the bacteria was determined by first manually specifying a line down the center of each bacterium using the "line" ROI tool in ImageJ (Abràmoff et al., 2004). The coordinates of the midpoint of this line were designated as the midline of the cell. The coordinates of each precinct were then transformed so that the origin was at the midline of the cell, and the y axis was aligned along the manually specified line. Following transformation, the Y coordinate of each precinct corresponds to its position along the length axis of the cell. To account for differences in the size of bacteria, precinct coordinates were normalized to the length of each cell. The distribution of precincts along the normalized length axis was then analyzed by aggregating precinct coordinates from 53 bacteria and calculating the relative frequency of Y precinct coordinates on either side of the midline.

Evaluation of Protein Synthesis by Pulse-Chase Labeling

The pulse-chase [^{35}S]-labeling assay was performed as described previously (Stubenrauch et al., 2016), except that *E. coli* BW25113 wild-type cells were, instead, treated with or without rifampicin (200 μg/mL) for 60 min to block or retain native transcription levels, respectively. Following a 10-min chase, samples were transferred directly to SDS loading dye and boiled for 10 min. Samples were analyzed by storage phosphor imaging (Stubenrauch et al., 2016) and immunoblotting for BamA (1:20,000), BamC (1:20,000), BamD (1:20,000), SurA (1:8,000), and DnaK (1:3,000).

Multiple Sequence Alignment of BamB Homologs

A previous study assessed BamB sequence diversity based on a curated set of 21 protein sequences (Albrecht and Zeth, 2011). Thus, these sequences were extracted from UniProt for a multiple sequence alignment using the Clustal Omega online tool (http://www.ebi.ac.uk/Tools/msa/clustalo/). The graphic was generated using Jalview (v2.10.1). The conserved columns with the highest score were indicated by "*" (score = 11). Columns with a score of 10 contain conservative alterations and were marked with a "+." The calculation were based on the analysis of multiply aligned sequences (AMAS) method of multiple sequence alignment analysis (Livingstone and Barton, 1993).

BamA *In Situ* Photocrosslinking

Crosslinking of BPA-containing BamA was conducted as before, using the BamA depletion strain (Daimon et al., 2017; Lehr et al., 2010), carrying pSup-BpaRS-6TRN and a pTnT-H6A2*bamA* (amber mutant) that expresses a His_6-BamA derivative from the native *bamA* promoter. After UV irradiation, the EMM fraction was isolated, and total EMM proteins were analyzed by SDS-PAGE and immunoblotting.

BamB *In Situ* Photocrosslinking

Stationary-phase cultures of *E. coli* BW25113 Δ*bamB*::Kan harboring pGEM-T-*bamBX-His*$_6$ and pSup-BpaRS-6TRN were grown in LB media supplemented with 1 mM BPA for 6 hr at 30°C with shaking (200 rpm). As described earlier, half of the *E.coli* culture was irradiated with UV (365 nm) for 10 min at room temperature (UV "+ "). Afterward, the heavy membrane was isolated by quick membrane preparation methods and then was analyzed by SDS-PAGE and immunoblotting.

BamB Disulfide Crosslinking

The protocol described previously (Noinaj et al., 2014) was used to identify disulfide crosslink formation in BamB mutants. Cultures grown to stationary phase were harvested by centrifugation (4,000 × *g*, 10 min, 4°C). The whole-cell lysates of cys-incorporated BamB mutants were resolved using SDS-PAGE under non-reducing conditions (no DTT), followed by immunoblotting with anti-BamB. To enhance disulfide crosslinking, cells were supplemented with 100 μM copper (II) sulfate and incubated at 37°C for 30 min with reaction buffer (20 mM Tris-HCl [pH 7.5] and 100 mM NaCl). To disrupt the disulfide bonds in the samples, a resuspended cell pellet in PBS was supplemented with 50 mM DTT and incubated for 30 min in RT. This suspension was then TCA-precipitated and resuspended in DTT-free loading buffer (2×) and analyzed by SDS-PAGE.

Identification of BamB-BamB Cross-linked Products by Mass Spectrometry

Bands corresponding to ~80 kDa and ~120 kDa were excised from SDS-PAGE gels (the same sizes detected in the corresponding western blot shown in Figure 4D) for the samples BamB($K^{90}C$) and BamB($D^{138}C$), respectively. A gel fragment from the same region in lane 1 derived using native BamB (see Figure 4D), in which no higher molecular weight cross-linked product was visible, was also excised and subjected to the same treatment and used as a negative control. Protein was reduced and alkylated prior to an in-solution overnight trypsin digestion (Promega, Madison, WI, USA).

Trypsin digests were analyzed by liquid chromatography-tandem mass spectrometry (LC-MS/MS), using the QExactive mass spectrometer (Thermo Scientific, Bremen, Germany) coupled online with a rapid separation liquid chromatography (RSLC)nano high-pressure liquid chromatography (HPLC) system (UltiMate 3000, Thermo Scientific, Bremen, Germany). Samples were concentrated on a 100-μm, 2-cm nanoViper PepMap 100 trap column with 95% buffer A (0.1% formic acid), at a flow rate of 15 μL/min. The peptides were then eluted and separated with a 50-cm Thermo RSLC PepMap 100 (internal diameter [i.d.], 75 μm; pore size, 100 Å) reversed-phase nano-column, with a 30-min gradient of 90% buffer A (0.1% formic acid) to 25 min of 30% buffer B (80% acetonitrile, 0.1% formic acid) and to 40% buffer B for 30 min, at a flow rate of 300 μL/min. The eluent was nebulized and ionized using the Thermo nano-electrospray source with a distal-coated fused silica emitter (New Objective, Woburn, MA, USA), with a capillary voltage of 1,900 V. Peptides were selected for MS/MS analysis in Full MS/dd-MS^2 (TopN) mode, with the following parameter settings: TopN 10; resolution, 17,500; MS/MS AGC target 1e5; 60-ms Max IT; NCE 27; and 3 m/z isolation window. Underfill ratio was at 10%, and dynamic exclusion was set at 15 s. Data from LC-MS/MS were exported to Mascot generic file format (*.mgf) using proteowizard 3.0.3631 (open source software; http://proteowizard.sourceforge.net) and searched against Swiss-Prot databases using the Mascot search engine (v2.4, Matrix Science, London, UK) with all taxonomy selected. The following search parameters were used: missed cleavages, 1; peptide mass tolerance, ±10 ppm Da; peptide fragment tolerance, ±0.02 Da; peptide charges, 2+, 3+, and 4+; fixed modifications, carbamidomethyl; variable modification, oxidation (Met).

Bacterial Membrane Microsomal Assay

Membrane preparation by a "classical method" was described previously (Dunstan et al., 2013). For the more rapid EMM method, *E. coli* cell pellets were resuspended in sonication buffer (50 mM Tris-HCl [pH 7.5], 150 mM NaCl, 5 mM EDTA) and disrupted by sonication on ice. The cell debris was removed by low-speed centrifugation (1,100 × g, 5 min, 4°C), and then the supernatant was centrifuged (15,000 × g, 10 min, 4°C). The resulting pellet, which represents the heavy membrane fraction, was resuspended in SEM buffer (250 mM sucrose, 10 mM MOPS-KOH [pH 7.2], 1 mM EDTA) and stored at −80°C until needed. To estimate the protein concentration in the heavy membrane fraction, 10 μL of membranes were mixed with 990 μL 0.6% w/v SDS and boiled for 5 min at 95°C. The optical density 280 (OD_{280}) of the mixture was subsequently taken: an OD_{280} reading of 0.21 corresponds to a protein concentration of 10 mg/mL.

To prepare [^{35}S]-labeled protein substrates, *in vitro* transcription by SP6-RNA polymerase and *in vitro* translation in rabbit reticulocyte lysate were performed as previously described (Chan and Lithgow, 2008). The heavy membrane fraction was resuspended with radiolabeled proteins in the membrane assembly buffer ([pH 7.2] 10 mM MOPS-KOH, 2.5 mM KH_2PO_4-K_2HPO_4, 250 mM sucrose, 15 mM KCl, 5 mM $MgCl_2$, 2 mM methionine, 5 mM DTT, 1% w/v BSA, 0.09% v/v Triton X-100) at 30°C for appropriate

periods. Assembly reactions were stopped by shifting on ice. The heavy membrane fraction was harvested by centrifugation (15,000 × *g*, 5 min, 4°C) and washed with SEM buffer. The proteins were analyzed by SDS-PAGE or BN-PAGE and storage phosphor imaging.

SUPPLEMENTAL INFORMATION

Supplemental Information includes Supplemental Experimental Procedures, seven figures, and seven tables and can be found with this article online at https://doi.org/10.1016/j.celrep.2018.04.093.

ACKNOWLEDGMENTS

The authors thank Bruker for access to the Vutara SR350 super-resolution system and, particularly, Carl Ebeling (Bruker) for assistance with the system. We thank Franz-Ulrich Hartl for expert advice on quantative proteomics, David Steer for expertise in protein mass spectrometry (Monash Biomedical Proteomics Facility), and Jonathan Wilksch for comments on the manuscript. This work was supported by the Multi-modal Australian Sciences Imaging and Visualisation Environment (MASSIVE; www.massive.org.au) and funded through an Australian Research Council (ARC) Laureate fellowship award (FL30100038), an ARC LIEF grant (LE150100110), and an NHMRC program grant (1092262). T.L. is an ARC Australian Laureate fellow, I.D.H. is an ARC Laureate postdoctoral fellow, and S.D.G. is the recipient of an ARC Laureate postgraduate research scholarship.

AUTHOR CONTRIBUTIONS

S.D.G., T.S., K.E.S., R.A.D., and C.J.S. designed and carried out analysis. A.J.F., I.D.H., C.T.W., T.N., and T.D.M.B. provided expertise to analyses. D.R.W. and T.D.M.B. provided expertise to building and optimizing the performance of the dSTORM instrument. I.D.H., K.E.S., C.T.W., A.J.F., T.D.M.B., K.D.E., and T.L. supervised experimental work and evaluated data. S.D.G., T.S., K.D.E., R.A.S., and T.L. wrote the manuscript.

DECLARATION OF INTERESTS

The authors declare no competing interests.

Received: October 31, 2017
Revised: March 5, 2018
Accepted: April 23, 2018
Published: May 29, 2018

REFERENCES

Abràmoff, M.D., Magalhães, P.J., and Ram, S.J. (2004). Image processing with ImageJ. Biophoton. Int. *11*, 36–42.

Albenne, C., and Ieva, R. (2017). Job contenders: roles of the β-barrel assembly machinery and the translocation and assembly module in autotransporter secretion. Mol. Microbiol. *106*, 505–517.

Albrecht, R., and Zeth, K. (2011). Structural basis of outer membrane protein biogenesis in bacteria. J. Biol. Chem. *286*, 27792–27803.

Almeida, J.G., Preto, A.J., Koukos, P.I., Bonvin, A.M.J.J., and Moreira, I.S. (2017). Membrane proteins structures: A review on computational modeling tools. Biochim. Biophys. Acta *1859*, 2021–2039.

Baba, T., Ara, T., Hasegawa, M., Takai, Y., Okumura, Y., Baba, M., Datsenko, K.A., Tomita, M., Wanner, B.L., and Mori, H. (2006). Construction of *Escherichia coli* K-12 in-frame, single-gene knockout mutants: the Keio collection. Mol. Sys. Biol. *2*, 2006.0008.

Bakelar, J., Buchanan, S.K., and Noinaj, N. (2016). The structure of the β-barrel assembly machinery complex. Science *351*, 180–186.

Bennion, D., Charlson, E.S., Coon, E., and Misra, R. (2010). Dissection of β-barrel outer membrane protein assembly pathways through characterizing BamA POTRA 1 mutants of *Escherichia coli*. Mol. Microbiol. *77*, 1153–1171.

Bergal, H.T., Hopkins, A.H., Metzner, S.I., and Sousa, M.C. (2016). The structure of a BamA-BamD fusion illuminates the architecture of the beta-barrel assembly machine core. Structure *24*, 243–251.

Chan, N.C., and Lithgow, T. (2008). The peripheral membrane subunits of the SAM complex function codependently in mitochondrial outer membrane biogenesis. Mol. Biol. Cell *19*, 126–136.

Clancy, B., and Cauller, L.J. (1998). Reduction of background autofluorescence in brain sections following immersion in sodium borohydride. J. Neurosci. Methods *83*, 97–102.

Daimon, Y., Iwama-Masui, C., Tanaka, Y., Shiota, T., Suzuki, T., Miyazaki, R., Sakurada, H., Lithgow, T., Dohmae, N., Mori, H., et al. (2017). The TPR domain of BepA is required for productive interaction with substrate proteins and the β-barrel assembly machinery (BAM) complex. Mol. Microbiol. *106*, 760–776.

Dunstan, R.A., Heinz, E., Wijeyewickrema, L.C., Pike, R.N., Purcell, A.W., Evans, T.J., Praszkier, J., Robins-Browne, R.M., Strugnell, R.A., Korotkov, K.V., and Lithgow, T. (2013). Assembly of the type II secretion system such as found in *Vibrio cholerae* depends on the novel Pilotin AspS. PLoS Pathog. *9*, e1003117.

Dunstan RA, Hay ID, Wilksch JJ, Schittenhelm RB, Purcell AW, Clark J, Costin A, Ramm G, Strugnell RA, Lithgow T. Mol Microbiol. 2015 Aug;97(4):616-29. https://doi.org/10.1111/mmi.13055.

Farrell, I.S., Toroney, R., Hazen, J.L., Mehl, R.A., and Chin, J.W. (2005). Photo-cross-linking interacting proteins with a genetically encoded benzophenone. Nat. Methods *2*, 377–384.

Gahlmann, A., and Moerner, W.E. (2014). Exploring bacterial cell biology with single-molecule tracking and super-resolution imaging. Nat. Rev. Microbiol. *12*, 9–22.

Gessmann, D., Chung, Y.H., Danoff, E.J., Plummer, A.M., Sandlin, C.W., Zaccai, N.R., and Fleming, K.G. (2014). Outer membrane β-barrel protein folding is physically controlled by periplasmic lipid head groups and BamA. Proc. Natl. Acad. Sci. USA *111*, 5878–5883.

Gu, Y., Li, H., Dong, H., Zeng, Y., Zhang, Z., Paterson, N.G., Stansfeld, P.J., Wang, Z., Zhang, Y., Wang, W., and Dong, C. (2016). Structural basis of outer membrane protein insertion by the BAM complex. Nature *531*, 64–69.

Hagan, C.L., Silhavy, T.J., and Kahne, D. (2011). β-Barrel membrane protein assembly by the Bam complex. Annu. Rev. Biochem. *80*, 189–210.

Han, L., Zheng, J., Wang, Y., Yang, X., Liu, Y., Sun, C., Cao, B., Zhou, H., Ni, D., Lou, J., et al. (2016). Structure of the BAM complex and its implications for biogenesis of outer-membrane proteins. Nat. Struct. Mol. Biol. *23*, 192–196.

Heuck, A., Schleiffer, A., and Clausen, T. (2011). Augmenting β-augmentation: structural basis of how BamB binds BamA and may support folding of outer membrane proteins. J. Mol. Biol. *406*, 659–666.

Ieva, R., Tian, P., Peterson, J.H., and Bernstein, H.D. (2011). Sequential and spatially restricted interactions of assembly factors with an autotransporter β domain. Proc. Natl. Acad. Sci. USA *108*, E383–E391.

Jansen, K.B., Baker, S.L., and Sousa, M.C. (2015). Crystal structure of BamB bound to a periplasmic domain fragment of BamA, the central component of the β-barrel assembly machine. J. Biol. Chem. *290*, 2126–2136.

Juette, M.F., Gould, T.J., Lessard, M.D., Mlodzianoski, M.J., Nagpure, B.S., Bennett, B.T., Hess, S.T., and Bewersdorf, J. (2008). Three-dimensional sub-100 nm resolution fluorescence microscopy of thick samples. Nat. Methods *5*, 527–529.

Kim, K.H., and Paetzel, M. (2011). Crystal structure of *Escherichia coli* BamB, a lipoprotein component of the β-barrel assembly machinery complex. J. Mol. Biol. *406*, 667–678.

Kim, K.H., Aulakh, S., and Paetzel, M. (2011). Crystal structure of β-barrel assembly machinery BamCD protein complex. J. Biol. Chem. *286*, 39116–39121.

Knowles, T.J., Browning, D.F., Jeeves, M., Maderbocus, R., Rajesh, S., Sridhar, P., Manoli, E., Emery, D., Sommer, U., Spencer, A., et al. (2011). Structure and function of BamE within the outer membrane and the β-barrel assembly machine. EMBO Rep. *12*, 123–128.

Lehr, U., Schütz, M., Oberhettinger, P., Ruiz-Perez, F., Donald, J.W., Palmer, T., Linke, D., Henderson, I.R., and Autenrieth, I.B. (2010). C-terminal amino

acid residues of the trimeric autotransporter adhesin YadA of *Yersinia enterocolitica* are decisive for its recognition and assembly by BamA. Mol. Microbiol. *78*, 932–946.

Leksa, N.C., and Schwartz, T.U. (2010). Membrane-coating lattice scaffolds in the nuclear pore and vesicle coats: commonalities, differences, challenges. Nucleus *1*, 314–318.

Li, B., Hu, Z., and Elkins, C.A. (2014). Detection of live *Escherichia coli* O157:H7 cells by PMA-qPCR. J. Vis. Exp. (*84*), e50967.

Livingstone, C.D., and Barton, G.J. (1993). Protein sequence alignments: a strategy for the hierarchical analysis of residue conservation. Comput. Appl. Biosci. *9*, 745–756.

Lycklama a Nijeholt, J.A., and Driessen, A.J. (2012). The bacterial Sec-translocase: structure and mechanism. Philos. Trans. R. Soc. Lond. B Biol. Sci. *367*, 1016–1028.

Malinverni, J.C., Werner, J., Kim, S., Sklar, J.G., Kahne, D., Misra, R., and Silhavy, T.J. (2006). YfiO stabilizes the YaeT complex and is essential for outer membrane protein assembly in *Escherichia coli*. Mol. Microbiol. *61*, 151–164.

Milenkovic, D., Blaza, J.N., Larsson, N.-G., and Hirst, J. (2017). The enigma of the respiratory chain supercomplex. Cell Metab. *25*, 765–776.

Miller, E.A. (2013). The COPII cage sharpens its image. Nat. Struct. Mol. Biol. *20*, 139–140.

Mlodzianoski, M.J., Juette, M.F., Beane, G.L., and Bewersdorf, J. (2009). Experimental characterization of 3D localization techniques for particle-tracking and super-resolution microscopy. Opt. Express *17*, 8264–8277.

Noinaj, N., Fairman, J.W., and Buchanan, S.K. (2011). The crystal structure of BamB suggests interactions with BamA and its role within the BAM complex. J. Mol. Biol. *407*, 248–260.

Noinaj, N., Kuszak, A.J., Gumbart, J.C., Lukacik, P., Chang, H., Easley, N.C., Lithgow, T., and Buchanan, S.K. (2013). Structural insight into the biogenesis of β-barrel membrane proteins. Nature *501*, 385–390.

Noinaj, N., Kuszak, A.J., Balusek, C., Gumbart, J.C., and Buchanan, S.K. (2014). Lateral opening and exit pore formation are required for BamA function. Structure *22*, 1055–1062.

Noinaj, N., Mayclin, S., Stanley, A., Jao, C., and Buchanan, S. (2016). From constructs to crystals - towards structure determination of β-barrel outer membrane proteins. J. Vis. Exp. (*113*), 53245.

Noinaj, N., Gumbart, J.C., and Buchanan, S.K. (2017). The β-barrel assembly machinery in motion. Nat. Rev. Microbiol. *15*, 197–204.

O'Neil, P.K., Rollauer, S.E., Noinaj, N., and Buchanan, S.K. (2015). Fitting the pieces of the beta-barrel assembly machinery complex. Biochemistry *54*, 6303–6311.

Plummer, A.M., and Fleming, K.G. (2016). From chaperones to the membrane with a BAM!. Trends Biochem. Sci. *41*, 872–882.

Rassam, P., Copeland, N.A., Birkholz, O., Tóth, C., Chavent, M., Duncan, A.L., Cross, S.J., Housden, N.G., Kaminska, R., Seger, U., et al. (2015). Supramolecular assemblies underpin turnover of outer membrane proteins in bacteria. Nature *523*, 333–336.

Rigel, N.W., Schwalm, J., Ricci, D.P., and Silhavy, T.J. (2012). BamE modulates the *Escherichia coli* beta-barrel assembly machine component BamA. J. Bacteriol. *194*, 1002–1008.

Sandoval, C.M., Baker, S.L., Jansen, K., Metzner, S.I., and Sousa, M.C. (2011). Crystal structure of BamD: an essential component of the β-barrel assembly machinery of Gram-negative bacteria. J. Mol. Biol. *409*, 348–357.

Seeger, M.A. (2017). Membrane transporter research in times of countless structures. Biochim. Biophys. Acta *1860*, 804–808.

Stenberg, F., von Heijne, G., and Daley, D.O. (2007). Assembly of the cytochrome bo3 complex. J. Mol. Biol. *371*, 765–773.

Strahl, H., and Errington, J. (2017). Bacterial membranes: structure, domains and function. Annu. Rev. Microbiol. *71*, 519–538.

Stubenrauch, C., Belousoff, M.J., Hay, I.D., Shen, H.-H., Lillington, J., Tuck, K.L., Peters, K.M., Phan, M.-D., Lo, A.W., Schembri, M.A., et al. (2016). Effective assembly of fimbriae in *Escherichia coli* depends on the TAM nanomachine. Nat. Microbiol. *1*, 16064.

Sundararaj, S., Guo, A., Habibi-Nazhad, B., Rouani, M., Stothard, P., Ellison, M., and Wishart, D.S. (2004). The CyberCell Database (CCDB): a comprehensive, self-updating, relational database to coordinate and facilitate in silico modeling of *Escherichia coli*. Nucleic Acids Res. *32*, D293–D295.

Ursell, T.S., Trepagnier, E.H., Huang, K.C., and Theriot, J.A. (2012). Analysis of surface protein expression reveals the growth pattern of the Gram-negative outer membrane. PLoS Comput. Biol. *8*, e1002680.

Vuong, P., Bennion, D., Mantei, J., Frost, D., and Misra, R. (2008). Analysis of YfgL and YaeT interactions through bioinformatics, mutagenesis, and biochemistry. J. Bacteriol. *190*, 1507–1517.

Wang, Y., Wang, R., Jin, F., Liu, Y., Yu, J., Fu, X., and Chang, Z. (2016). A supercomplex spanning the inner and outer membranes mediates the biogenesis of β-barrel outer membrane proteins in bacteria. J. Biol. Chem. *291*, 16720–16729.

Warren, G., and Dobberstein, B. (1978). Protein transfer across microsomal membranes reassembled from separated membrane components. Nature *273*, 569–571.

Webb, C.T., Selkrig, J., Perry, A.J., Noinaj, N., Buchanan, S.K., and Lithgow, T. (2012a). Dynamic association of BAM complex modules includes surface exposure of the lipoprotein BamC. J. Mol. Biol. *422*, 545–555.

Webb, C.T., Heinz, E., and Lithgow, T. (2012b). Evolution of the β-barrel assembly machinery. Trends Microbiol. *20*, 612–620.

Wiśniewski, J.R., and Rakus, D. (2014). Multi-enzyme digestion FASP and the 'Total Protein Approach'-based absolute quantification of the *Escherichia coli* proteome. J. Proteomics *109*, 322–331.

Wittelsberger, A., Mierke, D.F., and Rosenblatt, M. (2008). Mapping ligand-receptor interfaces: approaching the resolution limit of benzophenone-based photoaffinity scanning. Chem. Biol. Drug Des. *71*, 380–383.

Cell Reports, Volume *23*

Supplemental Information

The WD40 Protein BamB Mediates Coupling of BAM Complexes into Assembly Precincts in the Bacterial Outer Membrane

Sachith D. Gunasinghe, Takuya Shiota, Christopher J. Stubenrauch, Keith E. Schulze, Chaille T. Webb, Alex J. Fulcher, Rhys A. Dunstan, Iain D. Hay, Thomas Naderer, Donna R. Whelan, Toby D.M. Bell, Kirstin D. Elgass, Richard A. Strugnell, and Trevor Lithgow

SUPPLEMENTAL EXPERIMENTAL PROCEDURES

***d*STORM image acquisition.** SR images collected for the Alexa-647 labelled samples were illuminated continuously with 638 nm laser (70 mW) at an appropriate total internal reflection (TIRF) angle. After an initial period of < 30 s to drive dyes into the dark state, single molecule blinking time series were acquired for 10,000 frames at an exposure time of 20 ms and an electron multiplying (EM) gain of 50. Raw image pixel size with 100× objective and 1.6× magnifier engaged is 100 nm × 100 nm.

***d*STORM image processing.** The acquired data was reconstructed to super resolved images with an out-put pixel size of 10 nm using the open-source software rapi*d*STORM version 3.3.1 (Wolter et al., 2012). Full width of half maximum (FWHM) was set at 350 nm and blinks with a local signal-to-noise ratio (SNR) < 120 were discarded. Images were first colour coded for temporal appearance of blinks to detect sample drift, then (if applicable) corrected for drift using the linear drift correction available in rapi*d*STORM and exported as 8-bit greyscale images for further image processing. The corresponding localizations files for the SR images were extracted from rapi*d*STORM listing all detected localizations in x, y coordinates for quantification and data analysis.

3D single molecule localization microscopy setup. 3D STORM super-resolution imaging was performed on a Vutara SR 350 system (Bruker®) equipped with 4 imaging laser lines (488 nm, 560 nm, 640 nm and 750 nm, all 1 W laser power attenuated to 300 mW), one activation laser (405 nm, 100 mW), 60× oil immersion objective, sCMOS Hamatasu Camera Orca Flash 4.0 and quad field module (Orange/Red) for 3D imaging using the biplane approach (Juette et al., 2008; Mlodzianoski et al., 2009). Appropriate point spread function (PSF) calibration files were recorded at the start of each day using multi-color fluorescent beads.

3D STORM image acquisition. All dyes were first pumped into the dark state at a laser power of 11 kW/cm^2, the laser power was kept at 11 kW/cm^2 during the imaging process, individual dye molecules were reactivated with low amounts of 405 nm laser light (25 W/cm^2), 405 nm laser power was increased in 25 W/cm^2 intervals over the imaging time to keep the number of detected blinks at approximately the same level. One hundred frames were taken for each z-slice (2-3 z-steps), with 20-25 repeats at an exposure time of 10-20 ms.

3D STORM image processing. 3D super-resolution image reconstruction was performed using the Vutara 350 SRX Software, where the background threshold was set to 10, a confidence value of 0.8 and the particle size set to 50 nm diameter, which is approximated to the minimum size of primary-secondary antibody complexes. Images are coloured relevant to z-depth.

***d*STORM data processing and precinct analysis.** Analysis of the BAM complex super-resolution data was performed according to the method described by Owen *et al*., (2010). Molecule coordinates from each image were exported from rapi*d*STORM (Wolter et al., 2012) as a text file and imported into the statistical analysis environment R (Ihaka and Gentleman, 1996). These were used to generate Planar Point Pattern (PPP) objects using the *spatstat* package (Baddeley and Turner, 2005). A procedure of precinct analysis was performed in a Region of Interest (ROI) contained to membrane areas parallel to the cover slip to avoid 3D artefacts. ROIs were drawn on reconstructed super-resolution images using the polygon ROI tool in ImageJ (Abràmoff et al., 2004) and the coordinates of the polygon were exported to a tab-delimited file. ROI coordinates were then imported into R and used to create a polygonal *spatstat* window to isolate localizations falling within the ROI.

To analyze localizations in a given ROI, Ripley's K-function analysis was performed using the *spatstat Kest* function as:

Equation 1

$$\mathrm{K}(r) = \frac{1}{\lambda^2 A}\sum_{i=0}^{n}\ \sum_{j\neq i}^{n}\delta_{ij}e\left(x_i, x_j; r\right) \quad \text{where} \quad \delta_{ij} = \begin{cases} 1 & if \quad d_{ij} \le r \\ 0 & if \quad d_{ij} > r \end{cases}$$

where r is the spatial scale radius, A is the area of the analysis ROI, λ is the density of localizations, d_{ij} is the distance between two points i and j, and $e\left(x_i, x_j; r\right)$ is the edge-correction weighting. Ripley's isotropic edge-correction weighting, as implemented in the *spatstat* package, was used for all analyzes in this study.

The Ripley's K-function is defined such that $\lambda \mathrm{K}(r)$ gives the average number of localizations within a circle of radius, r, for a typical point in a point distribution. Under complete spatial randomness (or Poissonian distribution of points), the expected number of localizations within a circle of radius, r, is therefore given by $\lambda \pi r^2$ (i.e., the density of points multiplied by the area of the circle). Hence,

Equation 2

$$\mathrm{K}_{pois}(r) = \pi r^2$$

The scaling of K(r) is dependent upon the area of the enclosing circle (i.e., exponential with respect to r), therefore K(r) is often transformed to scale linearly with respect to r, yielding the L-function (also known as Besag's transformation):

Equation 3

$$L(r) = \sqrt{\frac{\mathrm{K}(r)}{\pi}}$$

Given **Equation 3**, random point distributions have an $L(r)$ equal to r at all values of r. Thus, $L(r)$ distributions in this study have been plotted as $L(r) - r$ versus r, where a random distribution coincides with the x-axis of the plot. A positive $L(r) - r$ value at a given r indicates clustering of localizations at that spatial scale, while a negative value indicates a regular distribution or spreading at that spatial scale. Peaks in the $L(r) - r$ distribution are spatial scales at which the highest precinct localization is observed. A $L(r) - r$ value equal to zero indicates a random distribution of points.

For the generation of precinct maps, localization data was explored using Getis and Franklin's local version of the Ripley's K-function (Getis and Franklin, 1987);

Equation 4

$$L(r)_i = \sqrt{\frac{A\sum_{j=0}^{n}\left(\frac{\delta_{ij}}{n}\right)e(x_j, y_j; r)}{\pi}} \quad \text{where} \quad \delta_{ij} = \begin{cases} 1 & if \quad d_{ij} \le r \\ 0 & if \quad d_{ij} > r \end{cases}$$

In our analyzes, a spatial scale r = 40nm was used for all analyzes. In order to resolve all precincts, this value was set below the r value at which the $L(r) - r$ distribution peaked in the overall Ripley's K analysis for BamC, BamA and other proteins described in this study.

A quantitative, pseudo-coloured precinct 'heat' map was then generated by interpolating a surface across the local $L(40)$ values in each analysis ROI using a 10 nm grid and 'v4' surface interpolation algorithm in Matlab. Heat-maps were thresholded at a $L(40)$ value of 69.28 to generate binary precinct maps. This threshold value equates to 3 times greater local molecular density at a spatial scale of r = 40 nm compared to a random distribution of points of the same density.

A marker assisted watershed transform was then used to split precincts that were touching each other ('clumped') using the watershed function of the *imager* R package. To determine markers for the watershed transform, a peak picking algorithm was developed to isolate the coordinates of localizations with peak $L(40)$ values i.e., those surrounded by the highest density of other localizations. Briefly, in order for a localization to be considered have a peak $L(40)$ value, its $L(40)$ value needed to exceed the threshold specified above by at least 10% and be greater than all other localizations within a circle of r = 24 nm. Following watershed splitting, objects smaller than 1000 nm² were excluded. Precinct density, nearest neighbor distances (i.e., the distance from the center of a precinct to the center of its nearest neighboring precinct) and the proportion of localizations inside precincts were measured using remaining objects. All precinct objects touching the ROI were excluded for measurements of precinct size and diameter, since these could be cropped by the ROI.

Source code for an automated version of the analysis procedure described here is hosted as a Git repository and is available at https://github.com/monashmicroimaging/autoclustr

SUPPLEMENTAL REFERENCES

Abràmoff, M.D., Magalhães, P.J., and Ram, S.J. (2004). Image processing with ImageJ. Biophot. Int. *11*, 36-42.

Albrecht, R. and Zeth, K. (2011) Structural basis of outer membrane protein biogenesis in bacteria. J Biol Chem. *286*, 27792-27803.

Baddeley, A., and Turner, R. (2005). spatstat: An R Package for Analyzing Spatial Point Patterns. 2005 *12*, 42.

Daimon, Y., Iwama, M.C., Tanaka, Y., Shiota, T., Suzuki, T., Miyazaki, R., Sakurada, H., Lithgow, T., Dohmae, N., and Mori, H. (2017). The TPR domain of BepA is required for productive interaction with substrate proteins and the β-barrel assembly machinery (BAM) complex. Mol. Micro. Sep 27. doi: 10.1111/mmi.13844.

Dunstan, R., Hay, I., Wilksch, J., Schittenhelm, R., Purcell, A., Clark, J., Costin, A., Ramm, G., Strugnell, R., and Lithgow, T. (2015). Assembly of the secretion pores GspD, Wza and CsgG into bacterial outer membranes does not require the Omp85 proteins BamA or TamA. Mol. Micro. *97*, 616-629.

Getis, A., and Franklin, J. (1987). Second-Order Neighborhood Analysis of Mapped Point Patterns. Ecology *68*, 473-477.

Ihaka, R., and Gentleman, R. (1996). R: a language for data analysis and graphics. J. Comp. Graph. Stats. *5*, 299-314.

Juette, M.F., Gould, T.J., Lessard, M.D., Mlodzianoski, M.J., Nagpure, B.S., Bennett, B.T., Hess, S.T., and Bewersdorf, J. (2008). Three-dimensional sub-100 nm resolution fluorescence microscopy of thick samples. Nat. Methods *5*, 527-529.

Mlodzianoski, M.J., Juette, M.F., Beane, G.L., and Bewersdorf, J. (2009). Experimental characterization of 3D localization techniques for particle-tracking and super-resolution microscopy. Opt. Express *17*, 8264-8277.

Okegawa, Y., and Motohashi, K. (2015). Evaluation of seamless ligation cloning extract preparation methods from an *Escherichia coli* laboratory strain. Analytical biochemistry *486*, 51-53.

Owen, D.M., Rentero, C., Rossy, J., Magenau, A., Williamson, D., Rodriguez, M., and Gaus, K. (2010). PALM imaging and cluster analysis of protein heterogeneity at the cell surface. J Biophot. *3*, 446-454.

Ryu, Y., and Schultz, P. (2006) Efficient incorporation of unnatural amino acids into proteins in *Escherichia coli*. Nat Methods. *3*, 263-265.

Wolter, S., Loschberger, A., Holm, T., Aufmkolk, S., Dabauvalle, M.C., van de Linde, S., and Sauer, M. (2012). rapidSTORM: accurate, fast open-source software for localization microscopy. Nat. Methods *9*, 1040-1041.

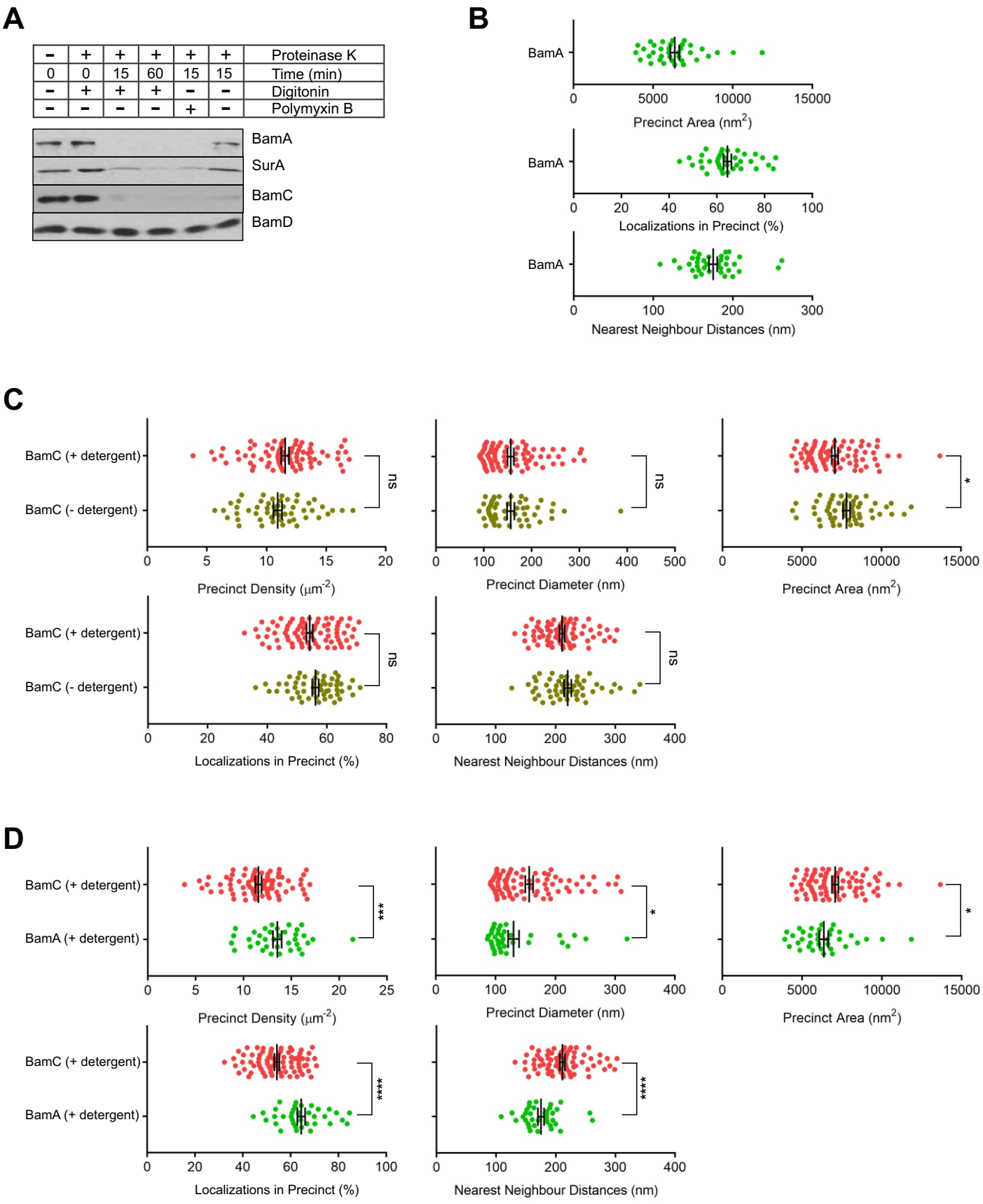
A
Proteinase K
Time (min)
Digitonin
Polymyxin B
BamA
SurA
BamC
BamD
B
BamA
Precinct Area (nm2)
Localizations in Precinct (%)
Nearest Neighbour Distances (nm)
C
BamC (+ detergent)
BamC (- detergent)
Precinct Density (µm-2)
Precinct Diameter (nm)
Precinct Area (nm2)
Localizations in Precinct (%)
Nearest Neighbour Distances (nm)
ns
*
D
BamC (+ detergent)
BamA (+ detergent)
Precinct Density (µm-2)
Precinct Diameter (nm)
Precinct Area (nm2)
Localizations in Precinct (%)
Nearest Neighbour Distances (nm)
***
****
*

Figure S1

Figure S1. Detergent treatments (proteinase K) and BamA and BamC distribution stats in detergent-treated *E. coli* cells. Related to Figure 1 and Table 1. (A) *E. coli* cells were incubated in buffer with or without 0.001% (w/v) digitonin (see Experimental Procedures), and Proteinase K was added for either 15 min or 60 min as indicated. Access of the protease into the periplasm was monitored by proteolysis of key marker proteins, after analysis of the samples by SDS-PAGE and immunoblotting. Antisera used recognize the following marker proteins: the protease-sensitive surface domains of BamC, the protease-sensitive (periplasmic) POTRA domains of BamA, and the protease-sensitive periplasmic chaperone SurA. As a loading control, the protease-insensitive periplasmic protein BamD was detected. To validate that membrane integrity was breached with the digitonin treatment, a replicate sample was treated instead with polymixin B, a validated compound for solubilizing the outer membrane to proteinase K. (B) Single-cell measurements of spatial parameters for BamA distribution in *E. coli* cells treated with 0.001% (w/v) digitonin. (C) Comparison of BamC distribution parameters where *E. coli* samples treated with or without 0.001% (w/v) digitonin are shown. (D) Samples of *E. coli* treated with 0.001% (w/v) digitonin were immunostained with either anti-BamC, or with an antibody raised to the POTRA domain of BamA. Comparisons of cluster parameters are shown for BamC and BamA. Comparisons of significance reported using unpaired t-test [(ns) $P > 0.05$, * $P \leq 0.05$, ** $P \leq 0.01$, *** $P \leq 0.001$, **** $P \leq 0.0001$)]. Error bars shown as mean ± SEM.

A

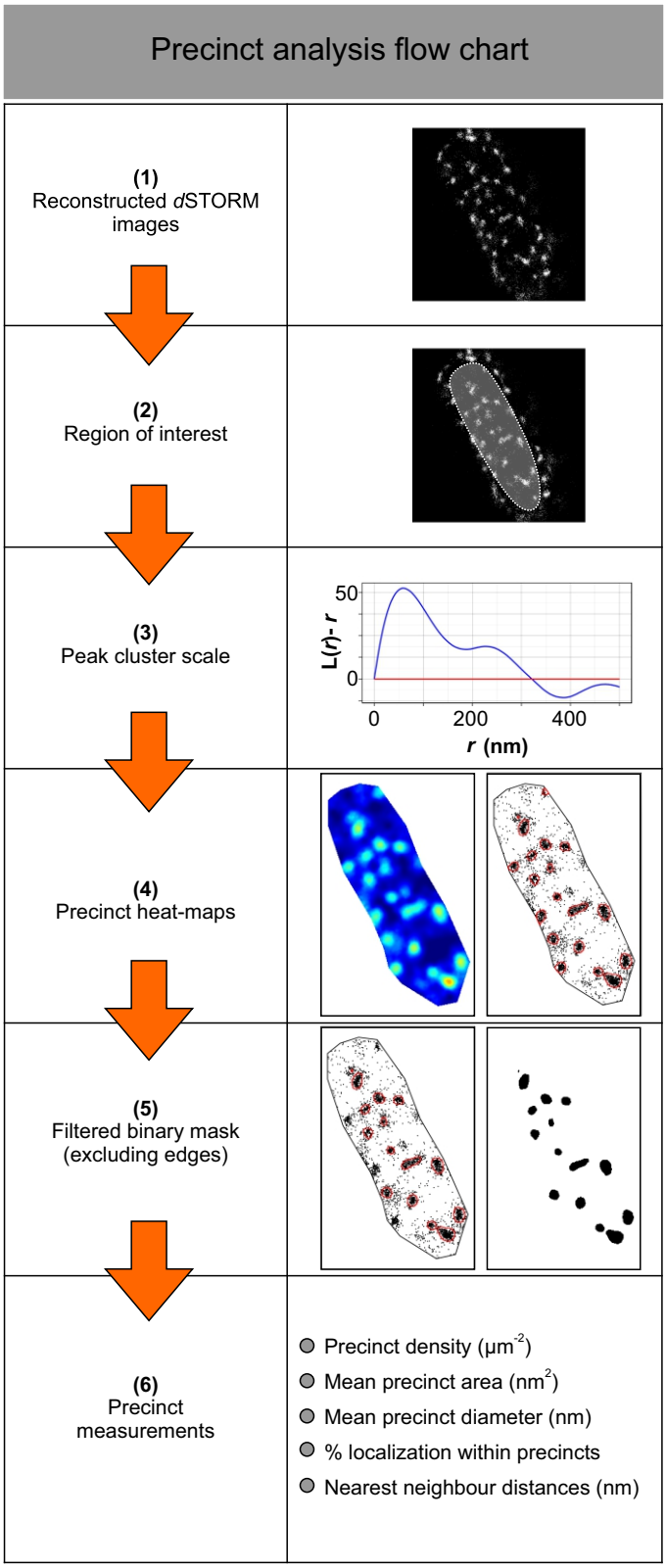
Precinct analysis flow chart
(1)
Reconstructed dSTORM
images
(2)
Region of interest
(3)
Peak cluster scale
50
L(r)- r
0
0
200
400
r (nm)
(4)
Precinct heat-maps
(5)
Filtered binary mask
(excluding edges)
(6)
Precinct
measurements
Precinct density (µm-2)
Mean precinct area (nm2)
Mean precinct diameter (nm)
% localization within precincts
Nearest neighbour distances (nm)

B

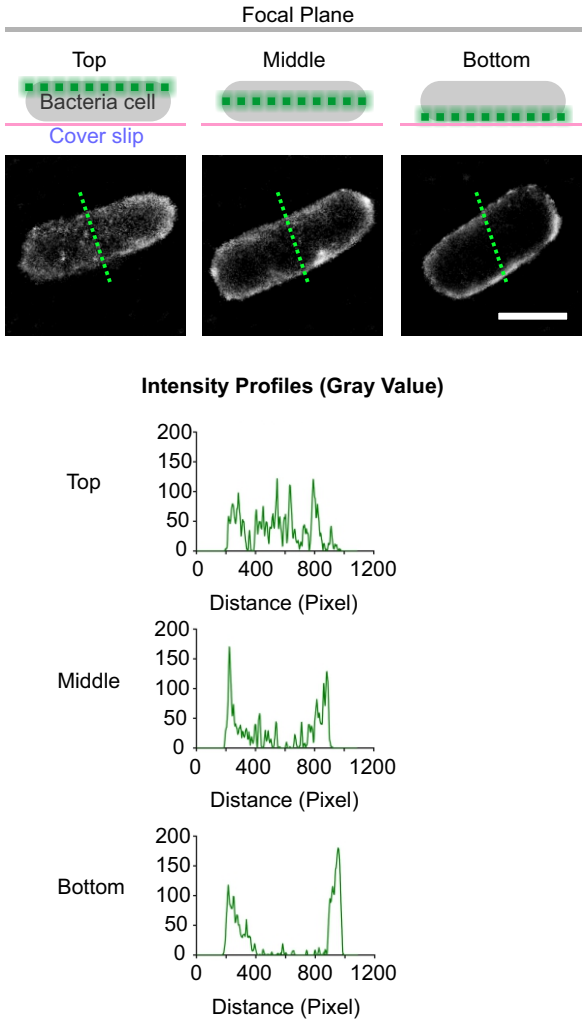
Focal Plane
Top
Middle
Bottom
Bacteria cell
Cover slip
Intensity Profiles (Gray Value)
Top
200
150
100
50
0
0
400
800
1200
Distance (Pixel)
Middle
Distance (Pixel)
Bottom
Distance (Pixel)

Figure S2

Figure S2. Methodology flow charts for topographical analysis. Related to Figure 1 and Figure 3. (A) Precinct analysis flow chart: [1] Bacteria *d*STORM image is reconstructed from the raw data using rapi*d*STORM software and all detected localizations are extracted. [2] A region of interest (ROI) is drawn excluding the outer edges to prevent edge effects due to the curvature of the bacterial cells. [3] From all localizations within the ROI a linear version of the Ripley's K function, L(r)-r vs r, is calculated and plotted against the radius r. [4] A heat map is generated over all localizations within the ROI. [5] Using adequate thresholding based on the L(r)-r vs r graph a mask is derived from the heat map. The mask is filtered for precincts at the edge of the ROI to exclude cropped precincts. [6] From the filtered mask additional precinct characteristics such as density, average precinct size, average precinct diameter, proportion of localizations within the precincts and nearest neighboring precinct distances can be calculated. Representative examples are shown for cells stained with anti-BamC and anti-BamA. (B) In preliminary independent assessments of *d*STORM imaging of *E. coli*, anti-Ag43 immunostained cells were used to optimize the detection of different focal planes of bacterial cells. Ag43 is an outer membrane protein of uniform distribution around the *E. coli* cell surface. Intensity profiles were generated for each focal plane (Left to right, Top, Middle and Bottom focal planes are shown). The highest average Gray values were acquired for Top focal plane, and were therefore used for all *d*STORM image analysis in this study. Scale bar 1 µm.

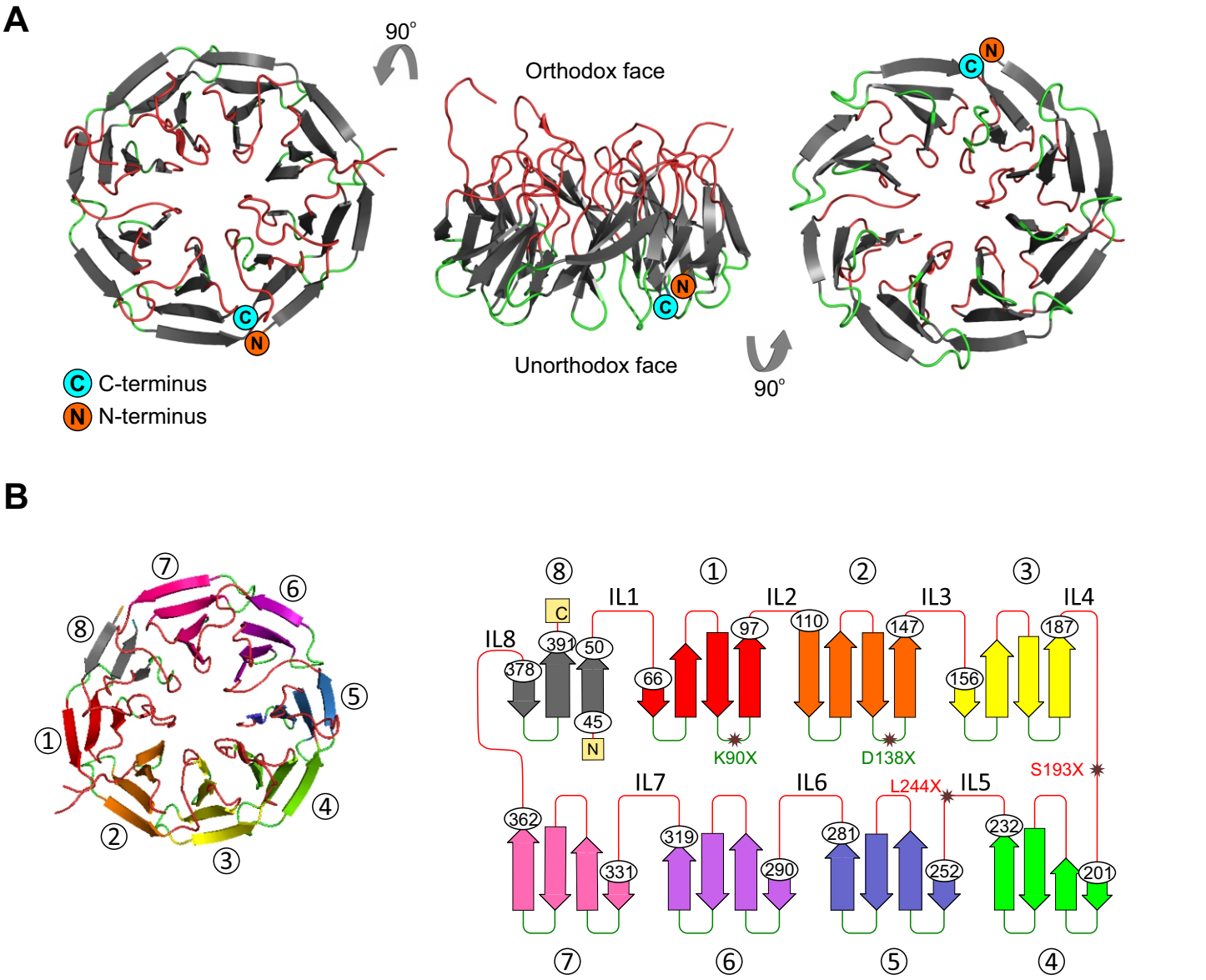
A
90°
Orthodox face
Unorthodox face
90°
C C-terminus
N N-terminus
B
IL1
IL2
IL3
IL4
IL8
IL7
IL6
IL5
K90X
D138X
L244X
S193X
C
N
C
α-BamA
α-BamB
BamB-BamA
BamA
(kDa)
UV
Orthodox face
Unorthodox face

Figure S3

Figure S3. Topology diagram and structural definition of the orthodox face and unorthodox face of BamB. Related to Figure 4. The disc-shaped WD40 protein BamB has two faces. The orthodox face is defined as that contacting BamA in the crystal structures of BamAB and BamABCDE. The other face is thereby the unorthodox face of BamB in terms of presumptive protein-protein interactions. (A) Crystal structure of BamB (PDB: 5ayw) showing orthodox (red) and unorthodox (green) facing loops. The N-terminus ("N") and C-terminus ("C") are highlighted. (B) BamB propeller structure with color coded blades (PDB: 5ayw) and topology diagram of BamB annotated to show the position of key residues (K^{90}, D^{138}, S^{193}, L^{244}) in the BPA alleles used for in situ cross-linking. (C) A total of 29 positions in BamB were mutated to accommodate BPA incorporation, and the resulting 29 strains of *E. coli* assayed for UV-dependent cross-linking into BamA. An SDS-PAGE immunoblot is shown documenting the results from probing with antibodies recognizing either BamA (upper panel) or BamB (lower panel). The position of the residues on either the orthodox or unorthodox face of BamB is color-coded as indicated.

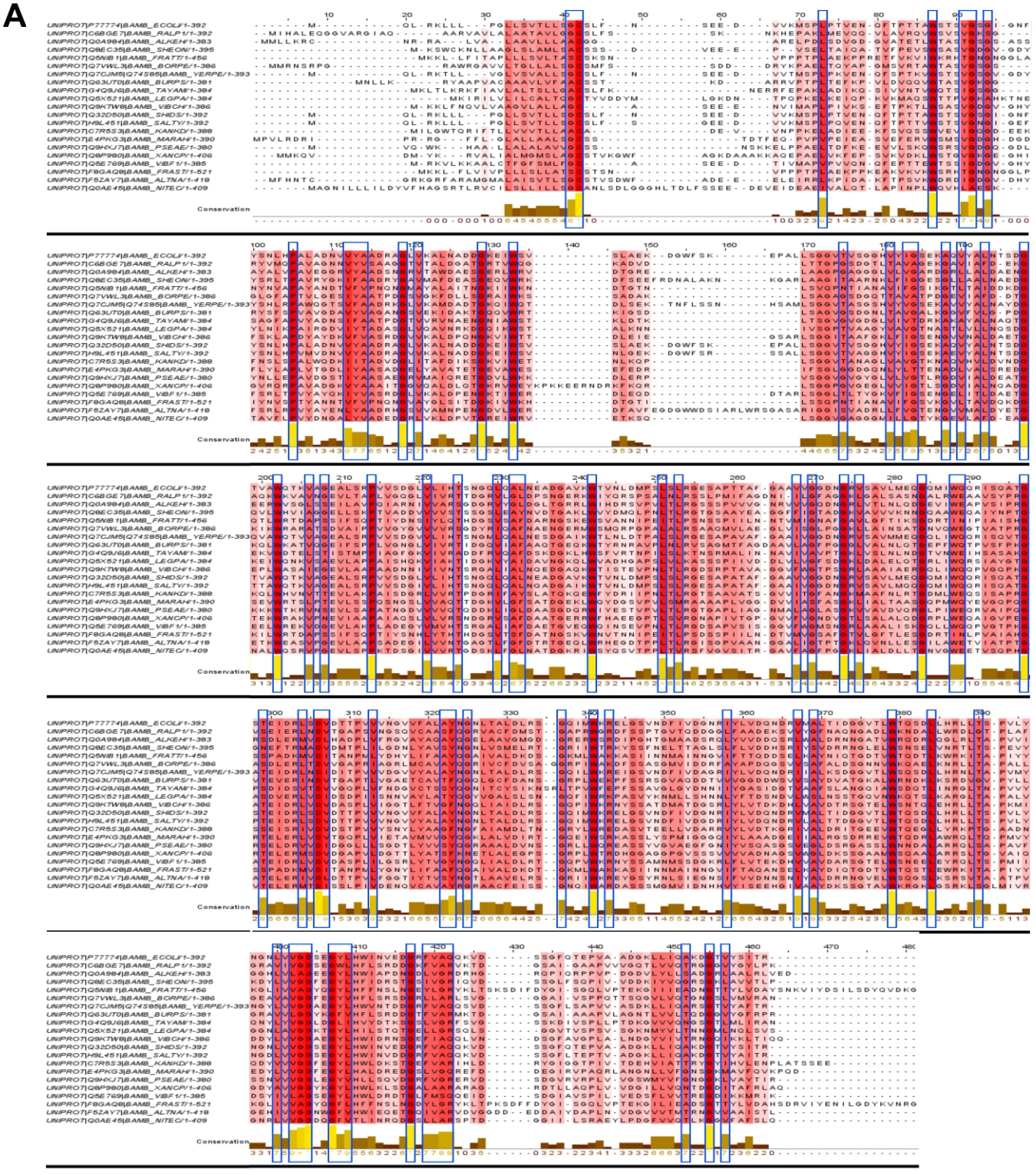
A
Conservation

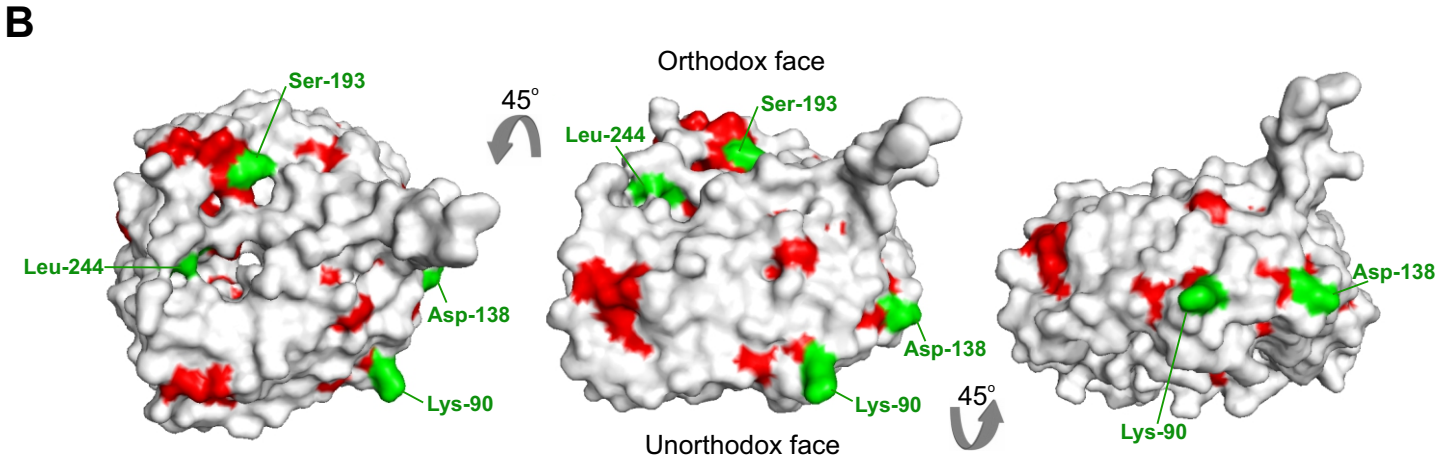
B
Orthodox face
Ser-193
45°
Leu-244
Ser-193
Leu-244
Asp-138
Asp-138
Lys-90
Lys-90
45°
Unorthodox face
Asp-138
Lys-90

Figure S4

Figure S4. Residue conservation of BamB homologs from different proteobacteria. Related to Figure 4. (A) Mutiple Sequence alignment of selected BamB proteins (Albrecht & Zeth, 2011). High to low conservation of residues were indicated from red to white in background. The conserved columns with the highest score were indicated by '*' (Score = 11). Columns with a score of 10 that contained mutations but all other properties were conserved, marked with a '+'. Residues with conservation scores ranging from 7-11 annotated in Blue boxes. Protein sequences were acquired from the Uniprot database; *Escherichia coli* (P77774), *Ralstonia pickettii* (C6BGE7), *Alkalilimnicola ehrlichii* (Q0A984), *Shewanella oneidensis* (Q8EC35), *Francisella tularensis* subsp. *Tularensis* (Q5NIB1), *Bordetella pertussis* (Q7VWL3), *Yersinia pestis* (Q7CJM5), *Burkholderia pseudomallei* (Q63UT0), *Taylorella asinigenitalis* (G4Q9J6), *Legionella pneumophila* (Q5X521), *Vibrio cholerae* (Q9KTW8), *Shigella dysenteriae* (Q32D50), *Salmonella typhimurium* (H9L451), *Kangiella koreensis* (C7R5S3), *Marinobacter adhaerens* (E4PKG3), *Pseudomonas aeruginosa* (Q9HXJ7), *Xanthomonas campestris* (Q8P980), *Vibrio fischeri* (Q5E769), *Francisella* sp. (F8GAQ8), *Alteromonas naphthalenivorans* (F5ZAY7), *Nitrosomonas eutropha* (Q0AE45). (B) Residues with conservation scores ranging from 7-11 were mapped onto BamB crystal structure (PDB: 3p1L) and indicated by red. Also indicated in green were the orthodox face residues Ser-193, Leu-244 and unorthodox face residues Lys-90, Asp-138.

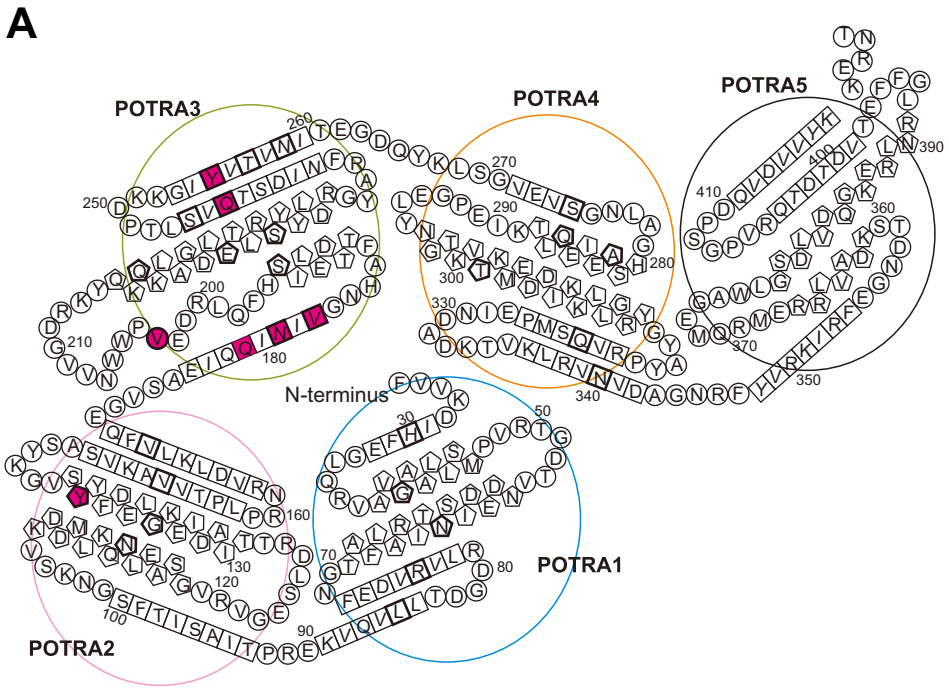
A
POTRA3
POTRA4
POTRA5
N-terminus
POTRA1
POTRA2

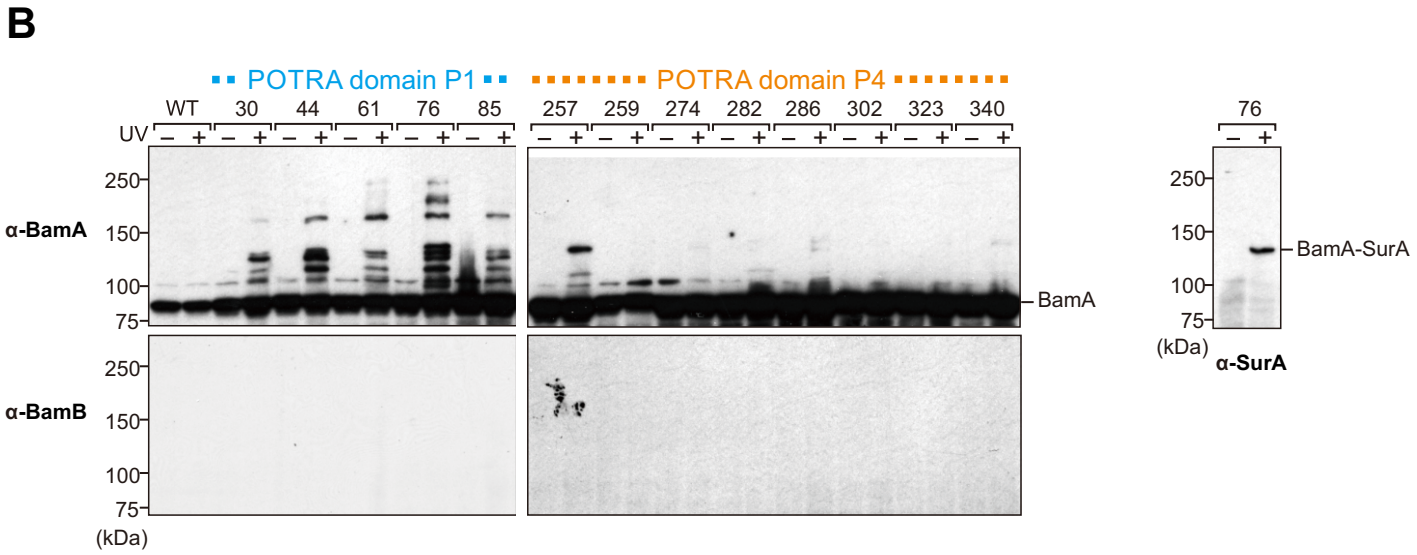
B
POTRA domain P1
POTRA domain P4
WT 30 44 61 76 85 257 259 274 282 286 302 323 340
UV
α-BamA
α-BamB
BamA
(kDa)
76
BamA-SurA
α-SurA

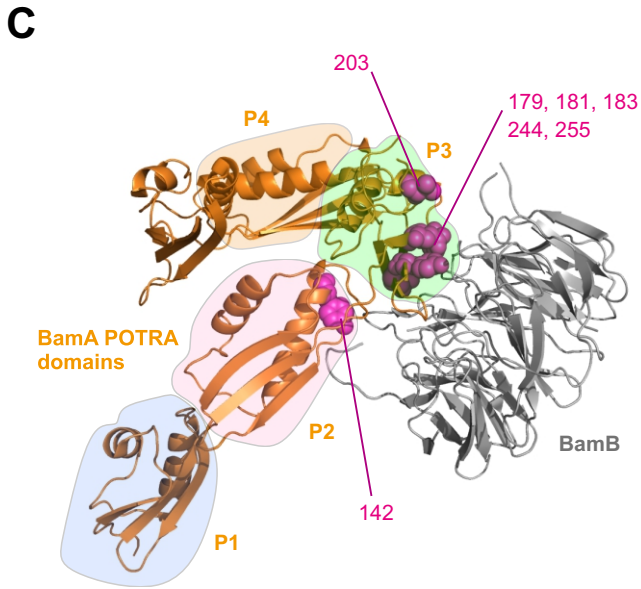
C
203
179, 181, 183
244, 255
P4
P3
BamA POTRA domains
P2
P1
BamB
142

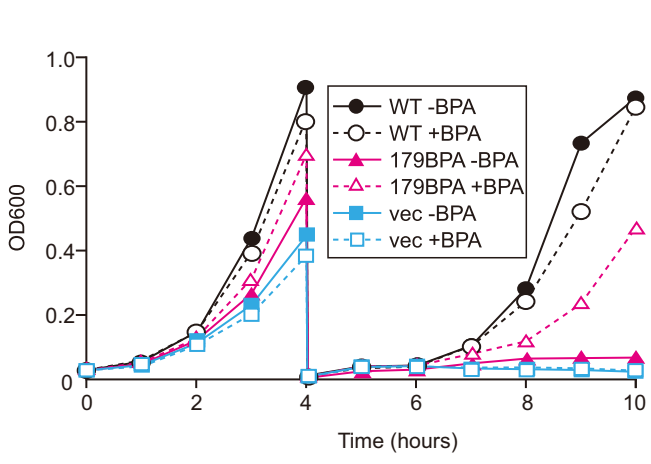
D
OD600
Time (hours)
WT -BPA
WT +BPA
179BPA -BPA
179BPA +BPA
vec -BPA
vec +BPA

Figure S5

Figure S5. BPA alleles of BamA. Related to Figure 4. (A) A schematic representation of the POTRA domains of BamA. In terms of secondary structure: circles, pentagons, and squares indicate residues in loops, α-helices, or β-strands, respectively. Residues where BPA was incorporated are labeled in bold, and those residues cross-linked to BamB are colored magenta. (B) BamA(BPA) alleles from positions POTRA domains P1 and P4. In each case, membrane samples were subjected to UV irradiation (+) or not (-), solubilized in detergent for nickel-affinity purification and then analyzed by SDS-PAGE and immunoblotting with antibodies specific for BamA, BamB or SurA. The migration of molecular weight standards is indicated in kDa. (C) Using the crystal structure of BamAB (pdb: 5ayw), residues where BPA was incorporated are mapped alleles from positions 30 to 168, which span POTRA domains P1 and P2, and BamA(BPA) alleles from positions 179 to 428 spanning POTRA domains P3 to P5. BamB crosslinked residues in POTRA domains of BamA are mapped onto the crystal structure BamAB (pdb: 5ayw) and are indicated by magenta. (D) Complementation of the BamA BPA mutants. BamA-depleted cells harboring pSup-BpaRS-6TRN and a pTnT- H6A2*bamA* derivative were cultivated overnight at 37°C in LB containing 0.2% arabinose, diluted 100-fold into LB-0.2% glucose medium supplemented with (solid lines) or without (dotted lines) 1 mM pBPA and grown at 37°C for 4 h. Cultures were then diluted 50-fold into the same medium, and cells were further grown at 37°C.

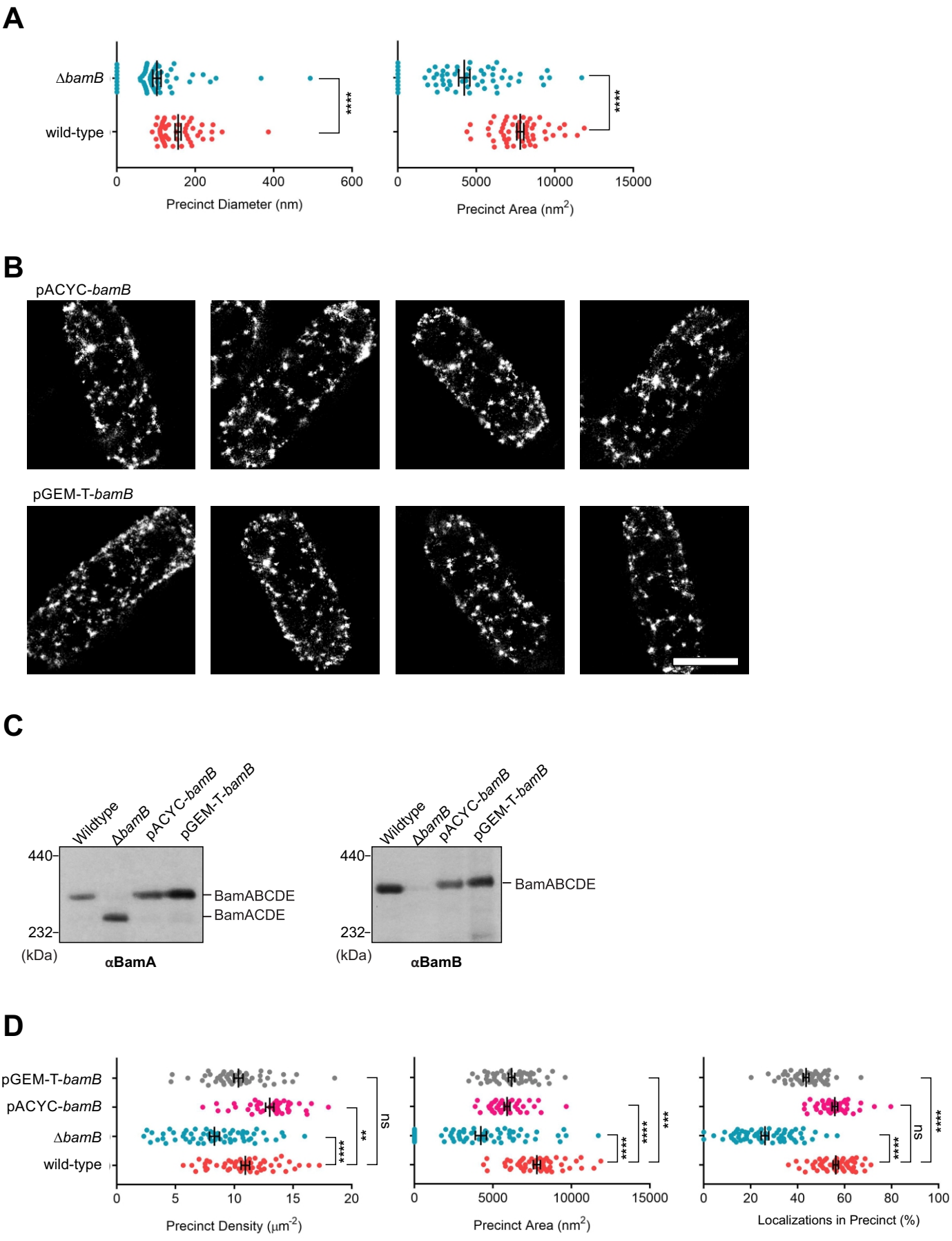
A
ΔbamB
wild-type
****
0
200
400
600
Precinct Diameter (nm)
****
0
5000
10000
15000
Precinct Area (nm2)
B
pACYC-bamB
pGEM-T-bamB
C
Wildtype
ΔbamB
pACYC-bamB
pGEM-T-bamB
440
232
(kDa)
BamABCDE
BamACDE
αBamA
Wildtype
ΔbamB
pACYC-bamB
pGEM-T-bamB
440
232
(kDa)
BamABCDE
αBamB
D
pGEM-T-bamB
pACYC-bamB
ΔbamB
wild-type
ns
**
****
0
5
10
15
20
Precinct Density (μm-2)
***
****
****
0
5000
10000
15000
Precinct Area (nm2)
ns
****
****
0
20
40
60
80
100
Localizations in Precinct (%)

Figure S6

Figure S6. Distribution parameters for the BAM complex in Δ*bamB* mutants. Related to Figure 5. (A) Spatial analysis for the BAM complex distribution in the Δ*bamB* mutants. Data for precinct diameter, precinct area and nearest neighbor distances are shown. Comparisons of significance reported using unpaired t-test [(ns) $P > 0.05$, **** $P \leq 0.0001$)]. (B) Complementation analysis was undertaken by *d*STORM imaging. Using anti-BamC staining to identify the BAM complex distribution, Δ*bamB* mutants that had been complemented with a *bamB* gene on either a pACYC plasmid or a pGEM-T plasmid. Scale bar 1 µm. The spatial distribution parameters for these samples (Table S6) do not differ significantly from the BAM complex distribution in wild-type *E. coli*. (C) Membrane extracts from wild-type *E. coli*, the isogenic Δ*bamB* mutant and the two complemented strains (Δ*bamB*, pACYC-*bamB* and pGEM-T-*bamB*) were subject to BN-PAGE and immunoblotting with antiserum recognizing BamA. The migration position for the molecular size markers is indicated. (D) Spatial analysis for the BAM complex distribution in the Δ*bamB* mutants, and the mutants expressing the complementing plasmid pACYC-*bamB* or pGEM-T-*bamB*. Comparisons of cluster parameters are shown for BamC and BamA. Comparisons of significance reported using unpaired t-test [(ns) $P > 0.05$, ** $P \leq 0.01$, *** $P \leq 0.001$, **** $P \leq 0.0001$)]. Error bars shown as mean ± SEM.

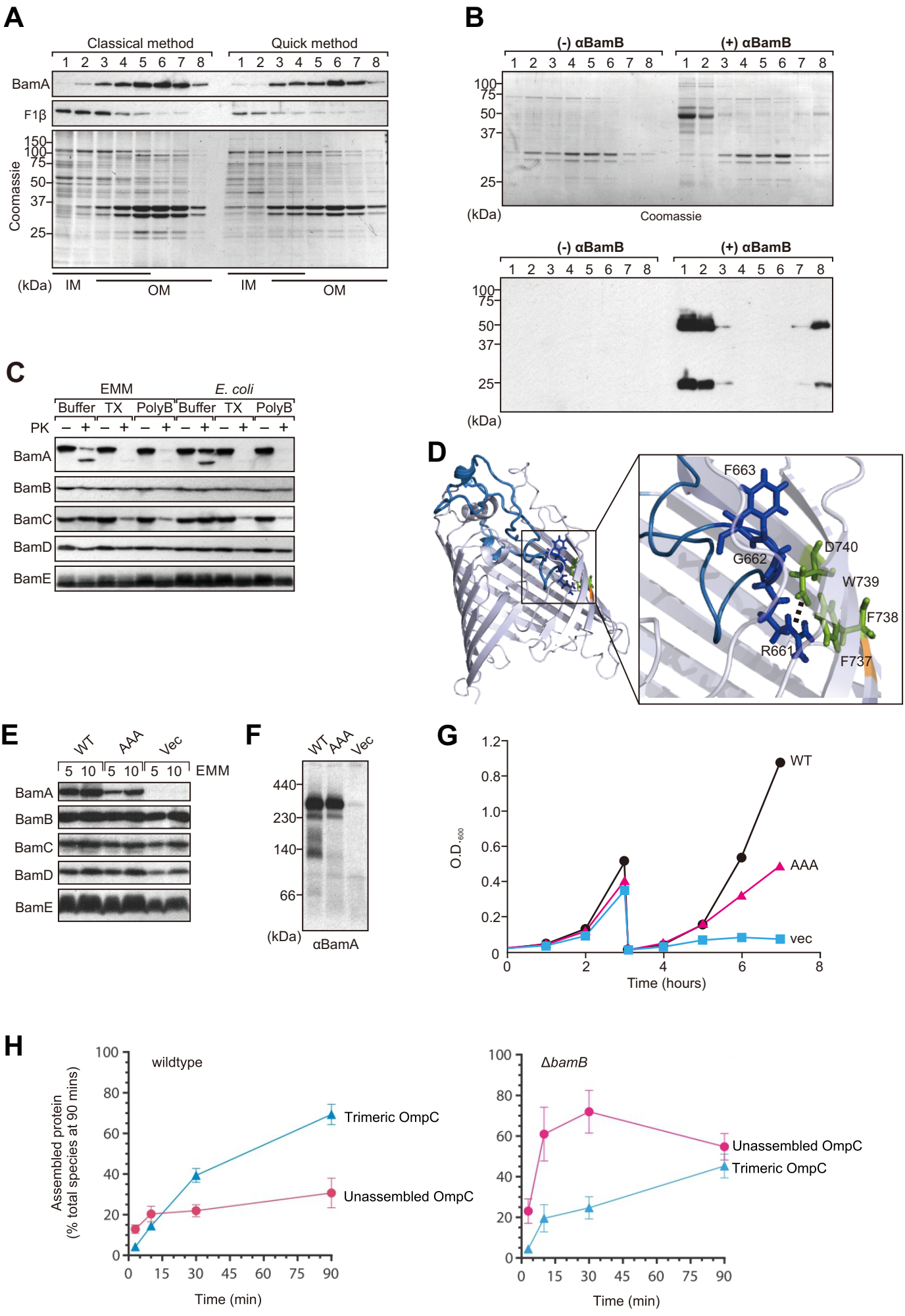
A
Classical method
Quick method
1 2 3 4 5 6 7 8
BamA
F1β
Coomassie
150
100
75
50
37
25
(kDa)
IM
OM
B
(-) αBamB
(+) αBamB
Coomassie
C
EMM
E. coli
Buffer TX PolyB Buffer TX PolyB
PK
BamA
BamB
BamC
BamD
BamE
D
F663
G662
D740
W739
F738
R661
F737
E
WT
AAA
Vec
5 10 5 10 5 10 EMM
F
440
230
140
66
αBamA
G
O.D.600
WT
AAA
vec
Time (hours)
H
wildtype
ΔbamB
Assembled protein
(% total species at 90 mins)
Trimeric OmpC
Unassembled OmpC
Time (min)

Figure S7

Figure S7. EMM assay to measure the assembly and trimerization of the major porin OmpC. Related to Figure 6. (A) Membranes were isolated by the "classical method" (Dunstan et al, 2015) or by the methodology optimized for the assembly-competent EMM, each method is described in the Experimental Procedures. In order to analyze the membranes in each fraction, they were subject to sucrose density centrifugation. Each fraction from the gradients was then analyzed by SDS-PAGE, followed by either immunoblotting with the indicated antibodies (upper panels) or staining with Coomassie blue (lower panel). The separation of inner and outer membranes and the overlapping fractions consisting of outer-inner membrane junctions are similar in both methods. (B) To determine the sidedness of the outer membranes, the EMM fraction was incubated with saturating amounts of antiserum raised to BamB (αBamB) on ice for 30 min, and then subjected to sucrose density centrifugation. Each fraction was analyzed by SDS-PAGE and Coomassie stain. The position of the ~50 kDa IgG heavy chain is indicated, as is the position of the ~30 kDa major porin OmpC. The outer membrane material that had the BamB protein presented on its surface ("inside-out" membranes) is of greater density when covered in IgG and migrates deeper into the gradient. Most of the outer membrane material does not bind αBamB, suggesting it is of "outside-out" topology. (C) To independently assess the topology of the outer membranes in the EMM fraction, EMM and intact *E. coli* were incubated without (-) or with (+) proteinase K (PK) in the presence (+) or absence (-) of the detergents Triton X-100 (TX) or polymyxin B (PolyB). Samples were analyzed by SDS-PAGE and immunoblotting to the indicated proteins. The characteristic fragmentation pattern of BamA seen in intact *E. coli*, where proteinase K cleaves a surface-exposed loop to generate a C-terminally truncated fragment of BamA, is largely mirrored in the EMM. This confirms that in the EMM fraction, the outer membranes are in an "outside-out" topology. Addition of 0.09% Triton X-100 is sufficient to allow the large proteinase K to enter the membranes and access the internal compartment, which is topologically the periplasmic face of the outer membrane. This is evident from the degradation of the BamA fragment and the protease-sensitive protein BamC. Like proteinase K, the detergent treatment is sufficient to allow access of substrate proteins such as OmpC to the periplasmic face of the BAM complex (Figure 6). (D) The crystal structure of BamAB (pdb: 5d0o) used to indicate the positions of mutated region of AAA mutant. Previous studies have shown that mutation of three highly-conserved residues within the loop (R^{661}, G^{662} and F^{663}) to three alanine residues severely effects BAM complex function. These three residues sit as an "RGF motif" in extracellular loop 6 of BamA. In the diagram, this loop6 is indicated in blue. Inset: detailed view of the interaction of RGF motif (blue) with residues F^{738} and D^{740} in the β-barrel wall of BamA (green and orange). (E) The steady-state levels of BAM complex subunits was determined in the EMM fraction prepared from the strains expressing wild-type *bamA* (WT), the AAA mutant of *bamA* (AAA) or the same expression plasmid without a *bamA* gene (vec). The EMM fractions were analyzed by SDS-PAGE and immunoblotting with the indicated antibodies. (F) The steady-state levels of the BAM complex was determined in the EMM fraction prepared from the strains expressing wild-type *bamA* (WT), the AAA mutant of *bamA* (AAA) or the same expression plasmid without a *bamA* gene (vec). The EMM fractions were solubilized with 1.0% DDM and subjected to BN-PAGE. The protein complexes were analyzed by immunoblotting with anti-BamA antibody. (G) Growth curve assessment of the *bamA*-depletion strain harboring pTnT-*bamA* (WT), pTnT-*bamA*AAA (AAA), or pTnT vector (vec, i.e. with no *bamA* gene) were cultivated overnight at 37°C in LB containing 0.2% arabinose, diluted 100-fold into LB-0.2% glucose medium and grown at 37°C for 3 h. Cultures were then diluted 50-fold into the same medium, and cells were further grown at 37°C. (H) OmpC assembly in the presence or absence of BamB was monitored over 90 minutes by BN-PAGE and storage phosphor imaging as per Fig. 6D. Autoradiographs were further analysed by densitometry from three independent experiments (n=3). Data is represented as the proportion of the indicated OmpC species at a given time-point relative to the total amount of OmpC species at the 90-minute time-point. For clarity, OmpC unfolded monomeric, folded monomeric and folded dimeric intermediate species were combined as "unassembled OmpC" intermediate species. Error bars represent SEM.

Supplemental Tables.

Table S1. Primary and secondary antibodies. Related to Figures 1, 2 and 3.

Antibody	**Type**	**Epitope source and specificity**	**Host**	**Source**
Anti-BamA	Polyclonal	Raised against *E. coli* BamA POTRA domain regions	Mouse	Gifted from S. Buchanan, NIH
Anti-BamA	Polyclonal	Raised against *E. coli* BamA	Rabbit	Laboratory stock
Anti-BamB	Polyclonal	Raised against *E. coli* BamB	Rabbit	Laboratory stock
Anti-BamC	Polyclonal	Raised against *E. coli* BamC	Mouse	Gifted from S. Buchanan, NIH
Anti-BamC	Polyclonal	Raised against *E. coli* BamC	Rabbit	Laboratory stock
Anti-BamD	Polyclonal	Raised against *E. coli* BamD	Rabbit	Laboratory stock
Anti-BamE	Polyclonal	Raised against *E. coli* BamE	Rabbit	Laboratory stock
Anti-Ag43(α)	Polyclonal	Raised against *E. coli* Ag43α Passenger domain	Rabbit	Gifted from M. Schembri, University of Queensland
Anti-LPS	Monoclonal	Raised against whole extracts of *E. coli* J5	Mouse	Abcam® ab35654
Anti-SurA	Polyclonal	Raised against *E. coli* SurA	Rabbit	Gifted from K. Tokatlidis, Glasgow University
Anti-MalE	Polyclonal	Raised against *E. coli* MalE	Rabbit	Laboratory stock
Anti-TamA	Polyclonal	Raised against *E. coli* TamA POTRA domain regions	Rabbit	Laboratory stock
Anti-OmpC	Polyclonal	Raised against *E. coli* OmpC	Rabbit	Laboratory stock
Anti-DnaK	Polyclonal	Cross-reactive, raised against mHsp70 (Ssc1) purified from *Saccharomyces cerevisiae*	Rabbit	Laboratory stock
Anti-F1-β	Polyclonal	Cross-reactive, raised against the F_1-β subunit of the ATPase purified from *Saccharomyces cerevisiae*	Rabbit	Laboratory stock
Goat anti-Rabbit IgG (H+L) Alexa Fluor® 647 conjugate.	Polyclonal	Rabbit IgG	Goat	ThermoFisher® A-21245
Goat anti-Mouse IgG (H+L) Alexa Fluor® 647 conjugate.	Polyclonal	Mouse IgG	Goat	ThermoFisher® A-21235

Table S2. Plasmids. Related to Experimental Procedures.

Plasmid name	Expressed Protein	Promoter	Vector backbone	Primers used	Cloning site/ method	Template DNA source/ Reference
pGEM-T-*bamB-His$_6$*	BamB-Cterm-His$_6$	Native	pGEM®-T Easy	SDG-BamB-Fw SDG-BamB-Rv	A-tailing	*E. coli*-K12 BW25113 genomic DNA
pGEM-T-*bamB(K90Bpa)-His$_6$*	BamB(K90Bpa)-Cterm-His$_6$	Native	pGEM®-T Easy	SDG-BamB-(K90Bpa)-Fw SDG-BamB-(K90Bpa)-Rv	Quick change mutagenesis	pGEM-T-*bamB-His$_6$*
pGEM-T-*bamB(D138Bpa)-His$_6$*	BamB(D138Bpa)-Cterm-His$_6$	Native	pGEM®-T Easy	SDG-BamB-(D138Bpa)-Fw SDG-BamB-(D138Bpa)-Rv	Quick change mutagenesis	pGEM-T-*bamB-His$_6$*
pGEM-T-*bamB(S193Bpa)-His$_6$*	BamB(S193Bpa)-Cterm-His$_6$	Native	pGEM®-T Easy	SDG-BamB-(S193Bpa)-Fw SDG-BamB-(S193Bpa)-Rv	Quick change mutagenesis	pGEM-T-*bamB-His$_6$*
pGEM-T-*bamB(L244Bpa)-His$_6$*	BamB(L244Bpa)-Cterm-His$_6$	Native	pGEM®-T Easy	SDG-BamB-(L244Bpa)-Fw SDG-BamB-(L244Bpa)-Rv	Quick change mutagenesis	pGEM-T-*bamB-His$_6$*
pGEM-T-*bamB(K90A)-His$_6$*	BamB(K90A)-Cterm-His$_6$	Native	pGEM®-T Easy	SDG-BamB(K90A)-Fw SDG-BamB(K90A)-Rv	Quick change mutagenesis	pGEM-T-*bamB-His$_6$*
pGEM-T-*bamB(K90S)-His$_6$*	BamB(K90S)-Cterm-His$_6$	Native	pGEM®-T Easy	SDG-BamB-(K90S)-Fw SDG-BamB-(K90S)-Rv	Quick change mutagenesis	pGEM-T-*bamB-His$_6$*
pGEM-T-*bamB(D138A)-His$_6$*	BamB(D138A)-Cterm-His$_6$	Native	pGEM®-T Easy	SDG-BamB-(D138A)-Fw SDG-BamB-(D138A)-Rv	Quick change mutagenesis	pGEM-T-*bamB-His$_6$*
pGEM-T-*bamB(D138S)-His$_6$*	BamB(D138S)-Cterm-His$_6$	Native	pGEM®-T Easy	SDG-BamB-(D138S)-Fw SDG-BamB-(D138S)-Rv	Quick change mutagenesis	pGEM-T-*bamB-His$_6$*
pGEM-T-*bamB(K90C)-His$_6$*	BamB(K90C)-Cterm-His$_6$	Native	pGEM®-T Easy	SDG-BamB-(K90C)-Fw SDG-BamB-(K90C)-Rv	Quick change mutagenesis	pGEM-T-*bamB-His$_6$*
pGEM-T-*bamB(D138C)-His$_6$*	BamB(D138C)-Cterm-His$_6$	Native	pGEM®-T Easy	SDG-BamB-(D138C)-Fw SDG-BamB-(D138C)-Rv	Quick change mutagenesis	pGEM-T-*bamB-His$_6$*
pGEM-T-*bamB(L192S,L194S,R195A)-His$_6$*	BamB(L192S,L194S,R195A)-Cterm-His$_6$	Native	pGEM®-T Easy	SDG-BamB-(triple mutant)-Fw SDG-BamB-(triple mutant)-Rv	Quick change mutagenesis	pGEM-T-*bamB-His$_6$*
pSup-BpaRS-6TRN	BpaRs and amber suppressor tRNA	N/A	N/A	N/A	N/A	Ryu and Schultz, 2006
pTnT-H6A2bamA	BamA-Nterm-His6Ala2	Native	pTnT			Daimon et al., 2017
pTnT-H6A2bamA(H30Bpa)	BamA(H30Bpa)-Nterm-His6Ala2	Native	pTnT	BamA30amb-f BamA30amb-r	Quick change mutagenesis	pTnT-H6A2bamA
pTnT-H6A2bamA(L44Bpa)	BamA(L44Bpa)-Nterm-His6Ala2	Native	pTnT	BamA44amb-f BamA44amb-r	Quick change mutagenesis	pTnT-H6A2bamA
pTnT-H6A2bamA(N61Bpa)	BamA(N61Bpa)-Nterm-His6Ala2	Native	pTnT	BamA61amb-f BamA61amb-r	Quick change mutagenesis	pTnT-H6A2bamA
pTnT-H6A2bamA(R76Bpa)	BamA(R76Bpa)-Nterm-His6Ala2	Native	pTnT	BamA76amb-f BamA76amb-r	Quick change mutagenesis	pTnT-H6A2bamA
pTnT-H6A2bamA(L85Bpa)	BamA(L85Bpa)-	Native	pTnT	BamA85amb-f	Quick change	pTnT-H6A2bamA

	Nterm-His6Ala2			BamA85amb-r	mutagenesis	
pTnT-H6A2bamA(T98Bpa)	BamA(T98Bpa)-Nterm-His6Ala2	Native	pTnT	BamA98amb-f BamA98amb-r	Quick change mutagenesis	pTnT-H6A2bamA
pTnT-H6A2bamA(K111Bpa)	BamA(K111Bpa)-Nterm-His6Ala2	Native	pTnT	BamA111amb-f BamA111amb-r	Quick change mutagenesis	pTnT-H6A2bamA
pTnT-H6A2bamA(N113Bpa)	BamA(N113Bpa)-Nterm-His6Ala2	Native	pTnT	BamA113amb-f BamA113amb-r	Quick change mutagenesis	pTnT-H6A2bamA
pTnT-H6A2bamA(G136Bpa)	BamA(G136Bpa)-Nterm-His6Ala2	Native	pTnT	BamA136amb-f BamA136amb-r	Quick change mutagenesis	pTnT-H6A2bamA
pTnT-H6A2bamA(Y142Bpa)	BamA(Y142Bpa)-Nterm-His6Ala2	Native	pTnT	BamA142amb-f BamA142amb-r	Quick change mutagenesis	pTnT-H6A2bamA
pTnT-H6A2bamA(V154Bpa)	BamA(V154Bpa)-Nterm-His6Ala2	Native	pTnT	BamA154amb-f BamA154amb-r	Quick change mutagenesis	pTnT-H6A2bamA
pTnT-H6A2bamA(V168Bpa)	BamA(V168Bpa)-Nterm-His6Ala2	Native	pTnT	BamA168amb-f BamA168amb-r	Quick change mutagenesis	pTnT-H6A2bamA
pTnT-H6A2bamA(Q179Bpa)	BamA(Q179Bpa)-Nterm-His6Ala2	Native	pTnT	BamA179amb-f BamA179amb-r	Quick change mutagenesis	pTnT-H6A2bamA
pTnT-H6A2bamA(N181Bpa)	BamA(N181Bpa)-Nterm-His6Ala2	Native	pTnT	BamA181amb-f BamA181amb-r	Quick change mutagenesis	pTnT-H6A2bamA
pTnT-H6A2bamA(V183Bpa)	BamA(V183Bpa)-Nterm-His6Ala2	Native	pTnT	BamA183amb-f BamA183amb-r	Quick change mutagenesis	pTnT-H6A2bamA
pMB11	TolC	T7 lac promoter	pET-15b	MB35-f MB36-r	NcoI/NdeI	*E. coli*-K-12 MG1655 genomic DNA
pCO2	Ag43	*ara* promoter	pBAD	N/A	N/A	Gifted from M. Schembri, University of Queensland
pTnT-BamB	BamB	*bamA* native	pTnT-H6A2bamA	BamBSL-f BamBSL-r	SLiCE (XbaI/SalI)	*E. coli*-K12 BW25113 genomic DNA

Table S3. Primers for plasmid constructs. Related to Figure 4.

Primer name	**Sequence 5'->3'**
SDG-BamB-Fw	CCATCAGGTTGATTCTGCACG
SDG-BamB-Rv	TTAGTGGTGATGGTGATGATGACGTGTAATAGAGTACACGGTTCC
SDG-BamB(K90A)-Fw	GCGGATGATGGCGCGGAAATCTGGTCT
SDG-BamB(K90A)-Rv	AGACCAGATTTCCGCGCCATCATCCGC
SDG-BamB-(K90S)-Fw	GCGGATGATGGCAGCGAAATCTGGTCT
SDG-BamB-(K90S)-Rv	AGACCAGATTTCGCTGCCATCATCCGC
SDG-BamB-(D138A)-Fw	CTGAATACCAGCGCGGGTACTGTGGCA
SDG-BamB-(D138A)-Rv	TGCCACAGTACCCGCGCTGGTATTCAG
SDG-BamB-(D138S)-Fw	CTGAATACCAGCAGCGGTACTGTGGCA
SDG-BamB-(D138S)-Rv	TGCCACAGTACCGCTGCTGGTATTCAG
SDG-BamB-(K90C)-Fw	GCGGATGATGGCTGCGAAATCTGGTCT
SDG-BamB-(K90C)-Rv	AGACCAGATTTCGCAGCCATCATCCGC
SDG-BamB-(D138C)-Fw	CTGAATACCAGCTGCGGTACTGTGGCATGG
SDG-BamB-(D138C)-Rv	CCATGCCACAGTACCGCAGCTGGTATTCAG
SDG-BamB-(triple mutant)-Fw	CCTTCGAGCTCTAGCGCGGGCGAGTCTGCGCCGACA
SDG-BamB-(triple mutant)-Rv	CGGCGCAGACTCGCCCGCGCTAGAGCTCGAAGGCATATC
MB35-f	TTTGACGTCCATGGGCAAGAAATTGCTCCCCATTCTTATC
MB36-r	GTTGACGTCATATGTCAGTTACGGAAAGGGTTATGAC
BamBSL-f	AACGCATAATAACGTCTAGAATGCAATTGCGTAAATTACTGCTGCCAGGACTGCTTTCCG
BamBSL-r	TTGCGGCCGCCCGGGTCGACCCTGTCCAGGAGCCGTTTTCAAAGTGAACGACAGAGACGA

Table S4. Primers for BPA introduction into BamB. Related to Figure 4.

Primer Names	Amber codon position	BamBX-Forward Primer (5'->3')	BamBX-Reverse Primer (5'->3')
SDG-BamB-(F42Bpa)-Fw & Rv	42	GTTGAAAACCAGTAGACGCCGACCACG	CGTGGTCGGCGTCTACTGGTTTTCAAC
SDG-BamB-(S51Bpa)-Fw & Rv	51	GCGTGGAGCACTTAGGTTGGTAGCGGC	GCCGCTACCAACCTAAGTGCTCCACGC
SDG-BamB-(S54Bpa)-Fw & Rv	54	ACTTCCGTTGGTTAGGGCATTGGCAAC	GTTGCCAATGCCCTAACCAACGGAAGT
SDG-BamB-(D69Bpa)-Fw & Rv	69	CCGGCACTGGCGTAGAACGTTGTCTAT	ATAGACAACGTTCTACGCCAGTGCCGG
SDG-BamB-(D87Bpa)-Fw & Rv	87	TTAGTAAAAGCGCTGAATGCGTAGGATGGCAAAGAAATCTGGTCT	AGACCAGATTTCTTTGCCATCCTACGCATTCAGCGCTTTTACTAA
SDG-BamB-(D88Bpa)-Fw & Rv	88	GTAAAAGCGCTGAATGCGGATTAGGGCAAAGAAATCTGGTCTGTC	GACAGACCAGATTTCTTTGCCCTAATCCGCATTCAGCGCTTTTAC
SDG-BamB-(G89Bpa)-Fw & Rv	89	AAAGCGCTGAATGCGGATGATTAGAAAGAAATCTGGTCTGTCAGC	GCTGACAGACCAGATTTCTTTCTAATCATCCGCATTCAGCGCTTT
SDG-BamB-(K90Bpa)-Fw & Rv	90	GCGGATGATGGCTAGGAAATCTGGTCT	AGACCAGATTTCCTAGCCATCATCCGC
SDG-BamB-(S94Bpa)-Fw & Rv	94	GGCAAAGAAATCTGGTAGGTCAGCCTGGCCGAG	CTCGGCCAGGCTGACCTACCAGATTTCTTTGCC
SDG-BamB-(E99Bpa)-Fw & Rv	99	GTCAGCCTGGCCTAGAAAGATGGCTGG	CCAGCCATCTTTCTAGGCCAGGCTGAC
SDG-BamB-(S137Bpa)-Fw & Rv	137	CAGGTTTACGCGCTGAATACCTAGGATGGTACTGTGGCATGGCAA	TTGCCATGCCACAGTACCATCCTAGGTATTCAGCGCGTAAACCTG
SDG-BamB-(D138Bpa)-Fw & Rv	138	CTGAATACCAGCTAGGGTACTGTGGCA	TGCCACAGTACCCTAGCTGGTATTCAG
SDG-BamB-(G139Bpa)-Fw & Rv	139	TACGCGCTGAATACCAGCGATTAGACTGTGGCATGGCAAACTAAA	TTTAGTTTGCCATGCCACAGTCTAATCGCTGGTATTCAGCGCGTA
SDG-BamB-(T140Bpa)-Fw & Rv	140	GCGCTGAATACCAGCGATGGTTAGGTGGCATGGCAAACTAAAGTC	GACTTTAGTTTGCCATGCCACCTAACCATCGCTGGTATTCAGCGC
SDG-BamB-(A142Bpa)-Fw & Rv	142	AATACCAGCGATGGTACTGTGTAGTGGCAAACTAAAGTCGCGGGT	ACCCGCGACTTTAGTTTGCCACTACACAGTACCATCGCTGGTATT
SDG-BamB-(S193Bpa)-Fw & Rv	193	ATGCCTTCGCTCTAGTTGCGTGGCGAG	CTCGCCACGCAACTAGAGCGAAGGCAT
SDG-BamB-(G196Bpa)-Fw & Rv	196	CTCTCTTTGCGTTAGGAGTCTGCGCCG	CGGCGCAGACTCCTAACGCAAAGAGAG
SDG-BamB-(D242Bpa)-Fw & Rv	242	TCTACCGAAATTTAGCGTCTGAGCGAT	ATCGCTCAGACGCTAAATTTCGGTAGA
SDG-BamB-(L244Bpa)-Fw & Rv	244	GAAATTGACCGTTAGAGCGATGTTGAC	GTCAACATCGCTCTAACGGTCAATTTC
SDG-BamB-(G293Bpa)-Fw & Rv	293	TTCATCGTCGACTAGAATCGCATCTAT	ATAGATGCGATTCTAGTCGACGATGAA
SDG-BamB-(R295Bpa)-Fw & Rv	295	GTCGACGGCAATTAGATCTATCTGGTC	GACCAGATAGATCTAATTGCCGTCGAC
SDG-BamB-(N334Bpa)-Fw & Rv	334	CCGGTGCTGTATTAGGGCAACCTGGTG	CACCAGGTTGCCCTAATACAGCACCGG
SDG-BamB-(E352Bpa)-Fw & Rv	352	TGGATTAACGTCTAGGATGGTCGTTTC	GAAACGACCATCCTAGACGTTAATCCA
SDG-BamB-(S364Bpa)-Fw & Rv	364	CAAAAAGTTGATTAGTCCGGTTTCCAG	CTGGAAACCGGACTAATCAACTTTTTG
SDG-BamB-(D375Bpa)-Fw & Rv	375	CCGGTTGCCGCTTAGGGCAAACTGCTG	CAGCAGTTTGCCCTAAGCGGCAACCGG

Table S5. Primers for BPA introduction into BamA-POTRA domains. Related to Figure 4.

Primer Name	Amber codon position (X)	BamABpa-Forward Primer (5'->3')	BamABpa-Reverse Primer (5'->3')
BamA30amb-f and r	30	GTAGTGAAAGATATTTAGTTCGAAGGCCTTCAG	CTGAAGGCCTTCGAACTAAATATCTTTCACTAC
BamA44amb-f and r	44	GTTGGTGCGGCCCTCTAGAGTATGCCGGTGCGC	GCGCACCGGCATACTCTAGAGGGCCGCACCAAC
BamA61amb-f and r	61	GATGAAGATATCAGTTAGACCATTCGCGCTCTG	CAGAGCGCGAATGGTCTAACTGATATCTTCATC
BamA76amb-f and r	76	AACTTTGAGGATGTTTAGGTCCTTCGTGATGGT	ACCATCACGAAGGACCTAAACATCCTCAAAGTT
BamA85amb-f and r	85	GATGGTGATACCCTTTAGGTTCAGGTAAAAGAA	TTCTTTTACCTGAACCTAAAGGGTATCACCATC
BamA113amb-f and r	113	GACATGCTGAAGCAATAGCTCGAGGCTTCTGGT	ACCAGAAGCCTCGAGCTATTGCTTCAGCATGTC
BamA136amb-f and r	136	GCCGATATCGAGAAATAGCTGGAAGACTTCTAC	GTAGAAGTCTTCCAGCTATTTCTCGATATCGGC
BamA142amb-f and r	142	CTGGAAGACTTCTACTAGAGCGTCGGTAAATAT	ATATTTACCGACGCTCTAGTAGAAGTCTTCCAG
BamA154amb-f and r	154	GCCAGCGTAAAAGCTTAGGTGACCCCGCTGCCG	CGGCAGCGGGGTCACCTAAGCTTTTACGCTGGC
BamA168amb-f and r	168	GTTGACCTAAAACTGTAGTTCCAGGAAGGTGTG	CACACCTTCCTGGAACTACAGTTTTAGGTCAAC
BamA179amb-f and r	179	TCAGCTGAAATCCAGTAGATTAACATTGTTGGT	ACCAACAATGTTAATCTACTGGATTTCAGCTGA
BamA181amb-f and r	181	GAAATCCAGCAAATTTAGATTGTTGGTAACCAT	ATGGTTACCAACAATCTAAATTTGCTGGATTTC
BamA183amb-f and r	183	CAGCAAATTAACATTTAGGGTAACCATGCTTTC	GAAAGCATGGTTACCCTAAATGTTAATTTGCTG
BamA195amb-f and r	195	ACCGACGAACTGATCTAGCATTTCCAACTGCGT	ACGCAGTTGGAAATGCTAGATCAGTTCGTCGGT
BamA203amb-f and r	203	CAACTGCGTGACGAATAGCCGTGGTGGAACGTG	CACGTTCCACCACGGCTATTCGTCACGCAGTTG
BamA217amb-f and r	217	CGTAAATACCAGAAATAGAAACTGGCGGGCGAC	GTCGCCCGCCAGTTTCTATTTCTGGTATTTACG
BamA224amb-f and r	224	CTGGCGGGCGACCTTTAGACCCTGCGCAGCTAC	GTAGCTGCGCAGGGTCTAAAGGTCGCCCGCCAG
BamA228amb-f and r	228	CTTGAAACCCTGCGCTAGTACTATCTGGATCGC	GCGATCCAGATAGTACTAGCGCAGGGTTTCAAG
BamA244amb-f and r	244	AACATCGACTCTACCTAGGTCAGTCTGACGCCA	TGGCGTCAGACTGACCTAGGTAGAGTCGATGTT
BamA246amb-f and r	246	GACTCTACCCAGGTCTAGCTGACGCCAGATAAA	TTTATCTGGCGTCAGCTAGACCTGGGTAGAGTC
BamA255amb-f and r	255	GATAAAAAAGGTATTTAGGTCACGGTGAACATC	GATGTTCACCGTGACCTAAATACCTTTTTTATC
BamA257amb-f and r	257	AAAGGTATTTACGTCTAGGTGAACATCACCGAA	TTCGGTGATGTTCACCTAGACGTAAATACCTTT
BamA259amb-f and r	259	ATTTACGTCACGGTGTAGATCACCGAAGGCGAT	ATCGCCTTCGGTGATCTACACCGTGACGTAAAT
BamA274amb-f and r	274	TCTGGCGTTGAAGTGTAGGGCAACCTTGCCGGG	CCCGGCAAGGTTGCCCTACACTTCAACGCCAGA
BamA282amb-f and r	282	CTTGCCGGGCACTCCTAGGAAATTGAGCAGCTG	CAGCTGCTCAATTTCCTAGGAGTGCCCGGCAAG
BamA286amb-f and r	286	TCCGCTGAAATTGAGTAGCTGACTAAGATCGAG	CTCGATCTTAGTCAGCTACTCAATTTCAGCGGA
BamA302amb-f and r	302	AACGGCACCAAAGTGTAGAAGATGGAAGATGAC	GTCATCTTCCATCTTCTACACTTTGGTGCCGTT
BamA323amb-f and r	323	GCCTATCCGCGCGTATAGTCGATGCCCGAAATT	AATTTCGGGCATCGACTATACGCGCGGATAGGC
BamA340amb-f and r	340	GTTAAATTACGTGTGTAGGTTGATGCGGGTAAC	GTTACCCGCATCAACCTACACACGTAATTTAAC

Table S6. Key statistical figures from assembly precinct analysis. Related to Supplemental Figures S1 and S2.

Sample	**Sample size (N)**	**Average precinct density (μm^{-2})**	**Average Mean precinct area (nm^2)**	**Average Mean precinct diameter (nm)**	**Average localization within precincts (%)**	**Average nearest neighbour distances (nm)**
BamA (0.001% digitonin)	46	13.54 ± 0.4	6363 ± 278.7	130.2 ± 9.1	64.45 ± 1.6%	175.3 ± 5.2
BamA (0.001% tritonX-100)	48	12.13 ± 0.4	7184 ± 289.3	155.8 ± 9.3	65.32 ± 1.6%	155.8 ± 9.3
BamC (no detergent)	53	10.94 ± 0.4	7801 ± 221.2	156.3 ± 7.5	56.22 ± 1.1%	220.4 ± 6.0
BamC (0.001% digitonin)	77	11.56 ± 0.3	7074 ± 202.5	156.3 ± 6.7	54.24 ± 1.1%	211.1 ± 4.2
BamC (0.001% tritonX-100)	42	11.10 ± 0.3	7582 ± 292.5	155.7 ± 10.2	53.70 ± 1.3%	212.4 ± 5.9
BamC (+ rifampicin)	42	14.65 ± 0.4	6303 ± 200.4	125.5 ± 6.2	68.01 ± 1.5%	173.2 ± 4.2
BamC (Δ*bamB*::Kan)	61	8.316 ± 0.4	4232 ± 353.7	102.2 ± 10.7	26.11 ± 1.6%	220.6 ± 16.0
BamC (Δ*bamB*::Kan, pACYC-Duet-*bamB)*	41	13.02 ± 0.4	5906 ± 180.9	117.5 ± 6	55.83 ± 1.1%	189.5 ± 4.6
BamC (Δ*bamB*::Kan, pGEM-T-*bamB-His*$_{6)}$	48	10.36 ± 0.4	6193 ± 205.3	117.3 ± 3.5	43.58 ± 1.2%	207.2 ± 6.0

± Standard Error of Mean (SEM)

Sample size, n > 40

Table S7. Proteomic analysis of BamB disulphide crosslinks. Related to Figure 4. Protein Mass Spectrometry analysis of samples BamB ($K^{90}C$) and BamB ($D^{138}C$) showed top hits for BamB. Various other proteins ranging from ~70-90 kDa were also detected and were found in both cys crosslinked samples and in the control (the region of the gel corresponding to the lane containing the native BamB extracts) with similar low abundance.

Sample	Protein Rank	Protein	Uniprot accession number	Mass (kDa)	[Log Prob]	Best Score	Total Intensity	Number of PSMs	Coverage %
BamB ($K^{90}C$)	**1**	**BamB**	**P77774**	**41.92**	**1369.98**	**1732.90**	**2313266562.0**	**657**	**94.13**
	2	KatE	P21179	84.16	629.44	1398.7	107637350.7	169	74.9
	3	Pnp	P05055	77.10	523.08	1254.5	78888735	134	72.29
	4	PflB	P09373	85.36	508.37	1084.9	46247079.6	117	76.05
	5	AceF	P06959	66.1	454.49	978.9	46002444.1	101	67.14
BamB ($D^{138}C$)	**1**	**BamB**	**P77774**	**41.92**	**3111.64**	**1799.00**	**30595297563.5**	**2380**	**98.47**
	2	MgtA	P0ABB8	99.47	832.73	1105.5	496275958.3	250	61.47
	3	FusA	P0A6M8	77.60	766.12	1400.2	278083515.7	171	78.41
	4	AlaS	P00957	96.03	739.08	1240.2	82999251.3	107	68.49
	5	FtsY	P10121	54.51	736.56	1570.8	497978520.4	158	87.93
BamB (native)	1	KatE	P21179	84.16	1944.07	1457.4	5103958190.3	948	88.31
	2	FusA	P0A6M8	77.60	737.35	1346.9	480143432.5	217	78.27
	3	ClpB	P63284	95.58	730.53	955.7	133518256.8	131	69.78
	4	BamA	P0A940	90.55	719.94	1354.5	223370310.9	148	75.56
	5	DnaK	P0A6Y8	69.11	711.55	1625.4	190318348.4	145	76.8

[Log Prob]: Absolute value of the Log base 10 of the protein p-value (p is the probability that the observed match is a random event). **Best Score** - Largest Byonic score of a Protein Spectral Match (PSM) assigned to the protein. **Total Intensity** – Sum of all fragment peak intensities over all MS/MS spectra. **Number of PSMs** - Total number of PSMs including duplicate PSMs. **Coverage %** – Percent of the protein sequence covered by PSMs.